PB-214 906

THE ROLE OF WAVES AND MONOMOLECULAR FILMS ON GAS ABSORPTION

Daniel Philip Boyd

Maryland University
College Park, Maryland

1965

DISTRIBUTED BY:

NTIS

National Technical Information Service
U. S. DEPARTMENT OF COMMERCE
5285 Port Royal Road, Springfield Va. 22151

WP-00323 Chin

PB 214 906

Department of Chemical Engineering
University of Maryland
College Park, Maryland

Reproduced by
NATIONAL TECHNICAL
INFORMATION SERVICE
U S Department of Commerce
Springfield VA 22151

THE ROLE OF WAVES AND MONOMOLECULAR FILMS ON GAS ABSORPTION

by

DANIEL PHILIP BOYD

Details of illustrations in this document may be better studied on microfiche

Ta

APPROVAL SHEET

Title of Thesis: THE ROLE OF WAVES AND MONOMOLECULAR FILMS ON GAS ABSORPTION

Name of Candidate: Daniel Philip Boyd
Master of Science, 1965

Thesis and Abstract Approved: _____
Joseph M. Marchello
Associate Professor
Chemical Engineering

Date Approved:

I b

VITA

Name: Daniel Philip Boyd.

Permanent address: 4605 College Avenue, College Park, Maryland.

Degree and date to be conferred: M.S., 1965.

Date of birth: March 6, 1941.

Place of birth: Clear Spring, Maryland.

Secondary education: Clear Spring High School, 1959.

Collegiate institutions attended	Dates	Degree	Date of Degree
University of Maryland	1959-1963	B.S.Ch.E.	June, 1963
University of Maryland	1963-1965	M.S.	June, 1965

Major: Chemical Engineering.

Minor: Mechanical Engineering.

Positions held: Research Fellow, Department of Chemical Engineering, University of Maryland, College Park, Maryland.

Chemical Engineer, E. I. duPont deNemours & Co., Wilmington, Delaware.

Chemical Engineer, The Pennsylvania Glass Sand Corp., Hancock, West Virginia.

I.V

ABSTRACT

Title of Thesis: THE ROLE OF WAVES AND MONOMOLECULAR FILMS ON GAS ABSORPTION

Daniel Philip Boyd, Master of Science, 1965

Thesis directed by: Professor Joseph M. Marchello
Dept Chem Eng U. Maryland.

An experimental program was undertaken to determine the effect of small surface waves on interfacial mass transfer in a carbon dioxide-water system. A surface active agent, n-hexadecanol, was used to determine the effect on mass transfer.

The literature was searched to discover previous interest on this topic, and this survey is presented. A mathematical model describing an effective diffusivity is presented for a clean surface case. A more general model is developed for the monolayer case. This hypothetical effective diffusivity in most cases is larger than the value for that of molecular diffusion, except in the no wave, monolayer case where the layer tends to dampen out natural convection effects, and the value of the diffusivity approaches that of the molecular value.

The model for the clean surface produces data that tend to show the presence of natural convection through a buoyant effect or the Marangoni instability principle. In all cases the effective diffusivity is considerably larger than the value for molecular diffusion. The effect of

I d

variation of liquid depth shows that as depth decreases, the value of the effective diffusivity also decreases. This points out that as the fluid ellipse of particles in secondary motion flattens under the wave surface, the action of natural convection is retarded.

In the monolayer case, the film on the liquid surface retards mass transfer. The values obtained for the effective diffusivity are smaller than those obtained for the clean surface case. This phenomena supports the Marangoni instability principle, since the perturbations in surface concentrations which cause the changes in surface tension were retarded by the presence of the monolayer. The limiting value of this effective diffusivity in the no wave case was nearly that of molecular diffusion. This indicates that the presence of the monolayer dampens natural convection in the liquid phase, removing most turbulent aspects of the diffusion coefficient. The presence of a monolayer retards absorption to a point of many practical applications.

THE ROLE OF WAVES AND MONOMOLECULAR FILMS ON GAS ABSORPTION

by
Daniel Philip Boyd

Thesis submitted to the Faculty of the Graduate School
of the University of Maryland in partial fulfillment
of the requirements for the degree of
Master of Science
1965

If

ACKNOWLEDGEMENT

Appreciation is extended to the Division of Water Supply and Polution Control of the United States Department of Health, Education, and Welfare for the support of this research under Public Health Service Grant #00323.

The author expresses his deep gratitude to Professor Joseph M. Marchello for his continued aid and encouragement.

TABLE OF CONTENTS

Chapter		Page
ACKNOWLEDGEMENT		ii
INTRODUCTION		1
I.	LITERATURE SURVEY	3
II.	MATHEMATICAL MODELS	8
III.	MASS TRANSFER EXPERIMENTS	26
IV.	ANALYSIS AND DISCUSSION	40
V.	CONCLUSION	60
APPENDIX A. - LISTING OF DATA AND TABULATED QUANTITIES		63
APPENDIX B. - MISCELLANEOUS FIGURES		70
NOMENCLATURE		75
LITERATURE CITED		78

LIST OF TABLES

Table		Page
4-1.	VALUES FOR D_w FOR CLEAN SURFACE	48
4-2.	VALUES FOR D_w FOR MONOLAYER, LARGE FILM RESISTANCE	54
4-3.	VALUES FOR D_w FOR MONOLAYER, SMALL FILM RESISTANCE	55
A-1.	CLEAN SURFACE, 1/4" LIQUID DEPTH	64
A-2.	CLEAN SURFACE, 1/2" LIQUID DEPTH	64
A-3.	CLEAN SURFACE, 1" LIQUID DEPTH	65
A-4.	CLEAN SURFACE, 2" LIQUID DEPTH	65
A-5.	CLEAN SURFACE, 2" LIQUID DEPTH, NO GAUZE DAMPERS	65
A-M1.	MONOMOLECULAR FILM, 0 CPM FREQUENCY	66
A-M2.	MONOMOLECULAR FILM, 400 CPM FREQUENCY	66
A-M3.	MONOMOLECULAR FILM, 600 CPM FREQUENCY	67
A-M4.	MONOMOLECULAR FILM, 800 CPM FREQUENCY	68
A-S1.	CARBON DIOXIDE SOLUBILITY DATA	69

LIST OF FIGURES

Figure		Page
2-1.	Reflected Problem of Carslaw and Jaegar	13
2-2.	Variation of Coordinates	17
2-3.	Coordinates used by Rohsenow and Choi	17
3-1.	Water Deaeration Apparatus	28
3-2.	Photograph of Overall Apparatus	29
3-3.	Mass Transfer Equipment	31
3-4.	Photograph of Ripple Tank	33
3-5.	Photograph of Volumetric Apparatus	35
4-1.	Typical Raw Data Plot	43
4-2.	Variation of Effective Diffusivity with Depth .	46
4-3.	Effect of Liquid Depth and Wave Frequency on D_w	51
4-4.	Influence of Monolayer on D_w - For Large Film Resistance	56
4-5.	Influence of Monolayer on D_w - For Small Film Resistance	57
B-1.	Ripple Tank Gas Volume	71
B-2.	Solubility of Carbon Dioxide	72
B-3.	Wavelength-Frequency Relationships	73
B-4.	Cam Motor Speed	74

INTRODUCTION

Mass transfer has long been one of the foremost topics of interest in chemical engineering; its applications are many and varied. Observers have noted in applications of mass transfer, particularly in a gas-liquid system, the occurance of waves at the transfer interface. An excellent example of these waves are those produced in a falling film evaporator, or those associated with motion of a liquid phase in a trough or pipe. The surface agitation of a fluid in a stirred tank has interested many investigators.

In all of these occurances of wave motion, no identical type of waves exist and wave reproducibility has usually not been a subject of interest, either because of the difficulty of obtaining this reproducibility or the decision of a type wave to study. This dissertation discusses a small moving surface wave produced by a wave generation system that can be accurately controlled to measure wave properties accurately.

An interest in correlating meaningful results leads to the development of a hypothetical effective diffusivity, which consists not only of molecular diffusion, but also that produced by the turbulent motion in the fluid phase. Data were obtained for the diffusivity as a function of the liquid phase depth on a clean liquid surface in a carbon dioxide-water system. The effect of a surface active agent

on the mass transfer diffusion coefficient was also determined for this system.

Subsequent chapters search the literature for previous interest in the subject and relate this information. A mathematical model is developed for the clean surface case and for the case when a monolayer of surface active agent is applied to the liquid surface. The results obtained for these cases are discussed, and the analysis used to produce effective diffusivity data is presented. The results that arise from this experimentation are summarized in the conclusion, and their effect on practical applications of chemical engineering are presented. Figures and Tables that pertain to general analysis are presented within the chapters, whereas, the data used to determine the effective diffusivity is presented in Appendix A, and various charts and graphs are given in Appendix B.

CHAPTER I

LITERATURE SURVEY

Many investigations of mass transfer have been made for flow down the side of a column such as occurs in a falling film evaporator. These studies have been pursued by a variety of investigators (14,18,25,43,46). More recent work has been concerned with flow of films over a sphere (14), and the diffusion in radial moving films (33). Isolated investigations have also been reported, such as films running over liquid jets (36,41) and theoretical explanations for oscillation in water as it flows in a slotted trough (27). Oscillating jets were a topic of interest for other investigators (1).

Bond and Donald (7) have studied the absorption of ammonia from a gas stream in a wetted wall column. Upon determining a minimum flow rate below which the film would break down and where there would be a considerable reduction in liquid area, a difference in surface tension between the point where the film breaks and the main bulk of the liquid was attributed to the Marangoni Instability Principle. Chiang and Toor (12) investigated interfacial resistances for short contact time in an oxygen-water system.

Investigations (19,20,31,32) concerning wave phenomena that occur in a concurrent air and water flow system have been made. Hanratty and Hershman (20) discussed conditions

and methods of initiation of roll waves in shallow water streams. Eddy formation in liquid films flowing down a smooth plate was a topic studied by Tailby and Portalski (44). Levich (30) discussed the theory of mass transfer in a vertical liquid film with a waved surface.

In these investigations the waves or ripples, as those in the falling film evaporator, caused a marked increase in mass transfer rates. Striba and Hurt (43) have shown that the increase in area due to ripples is not enough to cause the increased mass transfer. They proposed an unknown degree of turbulence as an explanation for this phenomena. There seems to be no specific references to methods of differentiating between area and hydrodynamic contributions in the mass transfer rate.

The nature of waves that have been observed by various investigators are usually of different character, and attempts to find waves which might be reproducible have been futile. However, Scriven and Pigford (41) observed standing waves on a stagnant surface near the liquid exit of a wetted wall in a rotating drum. Others (18,25) have observed roll waves in wetted wall columns. Different types of waves or ripples, as those in a stirred tank, have varied effect on mass transfer (17).

Mathematical models have been postulated to describe the behavior of films with wave motions. Scriven (40) developed an equation to describe the dynamic behavior at a liquid interface, and in another analysis (42) he presented a

simplified mathematical model to account for the mechanism supplying energy to interfacial turbulence. His model related the interfacial tension and concentration profiles near the surface to the interfacial turbulence levels.

Bird, Stewart, and Lightfoot (5) have pointed out the analogy of thermal convection to natural convection by density differences in undisturbed situations. The effect of a vibrating surface on natural convective mass transfer for a solid-gas interface was investigated by Lemlich and Levy (29).

A more recent investigation in which an attempt was made to improve reproducibility in studying mass transfer through a wave surface was made by Chapman (11). He investigated the absorption of carbon dioxide into a water surface on which a periodic wave was propagated. He found that experimental relationships between wave length and frequency agreed with those predicted by classical wave hydrodynamics. His apparatus developed frequencies up to 550 cycles per minute. Measurements were made for non-disturbed and waved surfaces and the values of diffusivities calculated. Because of his inability to accurately determine wave amplitudes, he found it difficult to correlate diffusivity value with wave properties.

Muenz (34) undertook a program to determine the effect of small surface waves on interfacial mass transfer. During his experimental investigations he developed a technique for determining wave properties accurately. Experiments

with various gases as the gas phase and water as the liquid phase were carried out by measuring the rate of gas transfer through generated standing surface waves. He found that a marked increase in mass transfer was observed over that predicted by molecular transfer. He related the increase to natural convection effects of buoyant motion, and to fluid motion due to the secondary drift of fluid particles.

During the course of the work described in this dissertation, it was necessary to determine certain physical properties. Of the literature searched, Othmer and Gilmont (35) and Brock and Bird (8) correlated surface tension and temperature based on critical properties. Furguson (16) was concerned about the effect of solute concentration on surface tension, and noted that changes of the order of one-half of one percent had been observed when water was saturated with air. Others (28) have devised methods for calculating the effect of small concentrations of gases on surface tension making use of van der Waal's constants. More recent observers (45) have presented dilute molecular diffusivity data for different systems including that of carbon dioxide and water. Finally the International Critical Tables (24) served as the main source of equilibrium solubility data.

A search of the literature located several references to studies of the effect of a surface active agent upon mass transfer. A few investigations (3,6,9) presented views on retardation of evaporation by monolayers. Harkins, Copeland, and Boyd (13,21) considered a monolayer as a superliquid

in two dimensions and discussed changes in a condensed monolayer by considering the viscosity effects of a liquid-solid phase in the monolayer. They also discussed an alcohol monolayer as a function of temperature, pressure, and viscosity.

The thermodynamics of films, their energy and entropy of formation, and the effect of extension and spreading of insoluble monolayers were discussed by Harkins, Young, and Boyd (22). The absolute rates of hetrogeneous reactions and the general theory of absorption were discussed by Kimball (26). Several articles (2,38) were devoted to the rate of evaporation of water through fatty acid, ester, and alcohol monolayers.

Various investigators have studied the effect of films on absorption in stirred tanks (17,23). They investigated the absorption of carbon dioxide by water in the presence of various film forming compounds, and showed that calculated energies of activation based on energies of hole formation in films, together with a simple collision theory, gave resistances in close agreement with observed values. They concluded that the interfacial mass transfer resistance phenomena can be explained by postulating an energy barrier and a hydrodynamic effect operating at the same time.

CHAPTER II

MATHEMATICAL MODELS

Clean Surface Shallow Wave Absorption Theory: The Fourier-Poisson heat transfer equation (5) is used in developing the model. In deriving this equation a control volume, V, of liquid is assumed with a surface area, S. The molar concentration of the absorbing gas is C, and θ represents time. The rate of accumulation of the absorbing gas in moles/hour is

$$\int_V \frac{\partial C}{\partial \theta} \, dV \tag{2-1}$$

and the flux: [out - in] equals

$$\int_S \bar{J} \cdot d\bar{A} \tag{2-2}$$

where $\bar{J}$ is the total flux vector at a point on the surface and

$$d\bar{A} = \bar{n} \cdot dS \tag{2-3}$$

where $\bar{n}$ is the vector normal to the surface at the point.

Conservation of mass requires that output - input = accumulation, or

$$- \int_S \bar{J} \cdot d\bar{A} = \int_V \frac{\partial C}{\partial \theta} \, dV \quad . \tag{2-4}$$

Assuming dilute solutions, then there are no bulk velocities due to the diffusion of the dilute component (the absorbing

gas), then

$$\bar{J} = \bar{J}_f + \bar{J}_d = \bar{v} \cdot C - D\nabla C \quad , \qquad (2\text{-}5)$$

which is a Fick's law representation with bulk flow by diffusion. $\bar{J}_f$ is the total surface flux of the absorbing gas due to the bulk flow, $\bar{J}_d$ the total surface flux due to molecular diffusion, $\bar{v}$ the bulk vector velocity, and D the molecular diffusivity of the solute. Substituting equation (2-5) into (2-4) results in equation (2-6).

$$- \int_S (\bar{v} \cdot C - D\nabla C) \cdot d\bar{A} = + \int_V \frac{\partial C}{\partial \theta} \, dV \quad . \qquad (2\text{-}6)$$

Applying the divergence theorem to the left side of equation (2-6) results in,

$$- \int_V \nabla \cdot (\bar{v} \cdot C - D\nabla C) \, dV = + \int_V \frac{\partial C}{\partial \theta} \, dV \quad , \qquad (2\text{-}7)$$

and where V is chosen small,

$$\frac{\partial C}{\partial \theta} + \nabla \cdot (\bar{v}C) - \nabla \cdot (D\nabla C) = 0 \quad . \qquad (2\text{-}8)$$

D is assumed constant for dilute solutions, and for an incompressible fluid

$$\nabla \cdot \bar{v} = 0 \qquad (2\text{-}9)$$

thus,

$$\frac{\partial C}{\partial \theta} + \bar{v}\nabla C = D\nabla^2 C \qquad (2\text{-}10)$$

which is the general diffusion equation for dilute, non-reacting, binary systems.

Reynolds (39) in a turbulent flow analysis divided the variables into a fluctuating and non-fluctuating component as such:

$$v = v + v' \tag{2-11}$$

$$C = C + C' \tag{2-12}$$

where v is the fluctuating part and v' the non-fluctuating portion.

Substitution of (2-11) and (2-12) into (2-10) yields

$$\frac{\partial (C+C')}{\partial \theta} + \nabla (v+v')(C+C') = D\nabla^2 (C+C') \quad . \tag{2-13}$$

It is possible to time average by the following rules:

$$\overline{f} = f, \ \overline{f'} = 0, \ \overline{ff'} = 0, \ \overline{f'g'} \neq 0 \tag{2-14}$$

where f and g are arbitrary properties.

Assuming stepwise continuity in the variables, averaging is carried out inside the differentation, and

$$\frac{\partial \overline{C}}{\partial \theta} + \nabla (\overline{v}C) + \nabla (\overline{v'C'}) = D\nabla^2 \overline{C} \tag{2-15}$$

where v is assumed zero since there exists no net motion in the control volume, then

$$\frac{\partial C}{\partial \theta} + \nabla (\overline{v'C'}) = D\nabla^2 \overline{C} \quad . \tag{2-16}$$

As usual practice, on eddy diffusivity, ε, will be defined by the relation

$$\nabla (\overline{v'C'}) = - \varepsilon \nabla^2 \overline{C} \tag{2-17}$$

and inserting this into equation (2-16) gives a form of Fick's second law:

$$\frac{\partial \overline{C}}{\partial \theta} = (\varepsilon+D)\ \nabla^2 \overline{C} \quad . \tag{2-18}$$

In the work described in this dissertation, $\frac{\partial^2 C}{\partial X^2}$ is negligible compared to $\frac{\partial^2 C}{\partial y^2}$ in the $\nabla^2 \overline{C}$ term, and choosing $D_w = \varepsilon + D$ to be consistant with Muenz (34) work we have

$$\frac{\partial C}{\partial \theta} = D_w \frac{\partial^2 C}{\partial y^2} \tag{2-19}$$

where D_w is termed an "effective diffusivity."

Since the absorbing material (carbon dioxide) penetrates to the tank bottom in long time periods, the third boundary condition used by Chapman (11) needs to be changed. He used

$$\frac{\partial C}{\partial \theta} = D_w \frac{\partial^2 C}{\partial y^2} \tag{2-20}$$

with boundary conditions,

$$C\ (0,y) = 0 \tag{2-21}$$

$$C\ (\theta,0) = C_i \tag{2-22}$$

$$C\ (\theta,\infty) = 0 \tag{2-23}$$

where y is the direction normal to the surface. This gives an error function solution (34).

In the present case, however, we need to use

$$\frac{\partial C}{\partial \theta} = D_w \frac{\partial^2 C}{\partial y^2} \tag{2-24}$$

with boundary conditions,

$$C\ (0,y) = 0 \qquad (2\text{-}25)$$

$$C\ (\theta,0) = C_i \qquad (2\text{-}26)$$

and

$$\frac{\partial C}{\partial y}\ (\theta,+h) = 0 \qquad (2\text{-}27)$$

where h is the liquid depth in terms of the coordinate system used by Chapman (11) and Muenz (34).

The solution to this problem is presented in Carslaw and Jaeger (10). Rather than fit the third boundary condition, Carslaw and Jaeger reflected the problem in terms of a second tank as shown in Figure 2-1. They employed these boundary conditions:

$$C\ (0,y) = 0 \qquad (2\text{-}28)$$

$$C\ (\theta,+h) = C_i \qquad (2\text{-}29)$$

$$C\ (\theta,-h) = C_i \quad . \qquad (2\text{-}30)$$

Thus at y = 0 they obtained,

$$\frac{\partial C}{\partial y}\ (\theta,0) = 0 \qquad (2\text{-}31)$$

and the solution from this analysis is:

$$C = C_i - \frac{4C_i}{\pi} \sum_{n=0}^{\infty} \frac{(-1)^n}{(2n+1)} e^{-\frac{D_w(2n+1)^2\pi^2\theta}{4h^2}} \cdot \cos\left[\frac{(2n+1)\pi y}{2h}\right] \quad . \qquad (2\text{-}32)$$

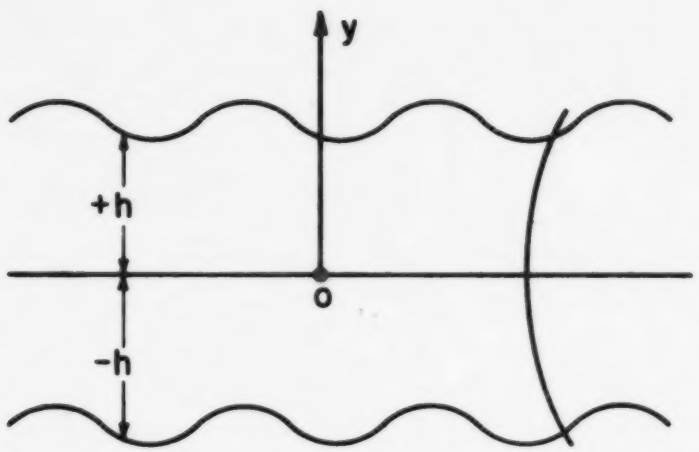

FIGURE 2-1 REFLECTED PROBLEM OF CARLSON AND JAEGAR.

The solution in equation (2-32) is the desired one, since reflection assumes that the third boundary condition is fulfilled at the center. The number of moles absorbed, Δn, is given by,

$$\Delta n = \int CdV = wl \int_0^h Cdy \qquad (2\text{-}33)$$

where (wl) = A,

then

$$\Delta n = C_i A \int_0^h \left\{ 1 - \frac{4}{\pi} \sum_{n=0}^{\infty} \frac{(-1)^n}{(2n+1)} e^{-\frac{D_w(2n+1)^2\pi^2\theta}{4h^2}} \cdot \cos\left[\frac{(2n+1)\pi y}{2h}\right] \right\} dy \quad , \qquad (2\text{-}34)$$

or

$$\Delta n = C_i A \left\{ \int_0^h dy - \frac{4}{\pi} \sum_{n=0}^{\infty} \frac{(-1)^n}{(2n+1)} e^{-\frac{D_w(2n+1)^2\pi^2\theta}{4h^2}} \cdot \int_0^y \cos\left[\frac{(2n+1)\pi y}{2h}\right] dy \right\} \quad . \qquad (2\text{-}35)$$

Integrating and evaluating the sine terms,

$$\Delta n = C_i A \left[h - \frac{8h}{\pi^2} \sum_{n=0}^{\infty} \frac{1}{(2n+1)^2} e^{-\frac{D_w(2n+1)^2\pi^2\theta}{4h^2}} \right] \qquad (2\text{-}36)$$

where $A\,h = V_{liquid}$, then

$$\Delta n = C_i V_l \left[1 - \frac{8}{\pi^2} \sum_{n=0}^{\infty} \frac{1}{(2n+1)^2} e^{-\frac{D_w(2n+1)^2\pi^2\theta}{4h^2}} \right] . \qquad (2\text{-}37)$$

Since $\Delta n_\infty = C_i V_1$ equals the total moles held by the liquid at saturation, and $\frac{\Delta n}{\Delta n_\infty}$ equals the fraction of saturation, then

$$\frac{\Delta n}{C_i V_1} = 1 - \frac{8}{\pi^2} \sum_{n=0}^{\infty} \frac{1}{(2n+1)^2} e^{-\frac{D_w (2n+1)^2 \pi^2 \theta}{4h^2}} \quad . (2\text{-}38)$$

By expanding the series and evaluating the respective terms using appropriate values for a normal analysis, such as 2×10^{-5} cm^2/sec for D_w at h = 2 cm and a time of 1800 sec, it was found that the second term was much less than the first, and the model becomes:

$$\frac{\Delta n}{C_i V_1} \approx 1 - \frac{8}{\pi^2} e^{-\frac{D_w \pi^2 \theta}{4h^2}} \quad . \qquad (2\text{-}39)$$

The percent unsaturation equals

$$\left[1 - \frac{\Delta n}{C_i V_1}\right] = \frac{8}{\pi^2} e^{-\frac{D_w \pi^2 \theta}{4h^2}} \qquad (2\text{-}40)$$

and taking the log of both sides, (2-41) is obtained.

$$\ln \left[1 - \frac{\Delta n}{C_i V_1}\right] = \ln \frac{8}{\pi^2} - \frac{D_w \pi^2 \theta}{4h^2} \quad . \qquad (2\text{-}41)$$

A plot of $\left[1 - \frac{\Delta n}{C_i V_1}\right]$ versus θ on semilog paper will give a slope of,

$$- \frac{D_w \pi^2}{4h^2} \quad ,$$

thus the value of D_w can be found by measuring the slope of

such a plot.

The Monolayer Absorption Model: The variation of the concentration of absorbed gas in the film and water is shown in Figure 2-2. With concentration increasing to the right, it is assumed that the gas is less soluable in the layer than in the water. The equation for the concentration gradient flux can be written:

$$N = \frac{D_f}{\delta} (C_{sf} - C_{sw}) = - D_w \frac{\partial C}{\partial y} (\theta, \delta) \qquad (2\text{-}42)$$

where C_{sf} is the saturation concentration in the film, and C_{sw} is the saturation concentration in the water. A discussion of the solution of the conduction equation with a film resistance at the surface is presented in Rohsenow and Choi (37) in terms of the drying of solids. The mathematics presented is similar, once the change from heat to mass transfer nomenclature is made. The coordinates used by Rohsenow and Choi are shown in Figure 2-3.

At equilibrium ($\theta = \infty$), it is assumed that the gas concentration in the monolayer may be expressed by:

$$P = H \overline{C} \qquad (2\text{-}43)$$

where $\overline{C}$ is the concentration of carbon dioxide in the monolayer, P the gas pressure, and H a Henry's law constant. Likewise at equilibrium, the distribution of gas between the layer and the water is represented by:

$$C = m \overline{C} \qquad (2\text{-}44)$$

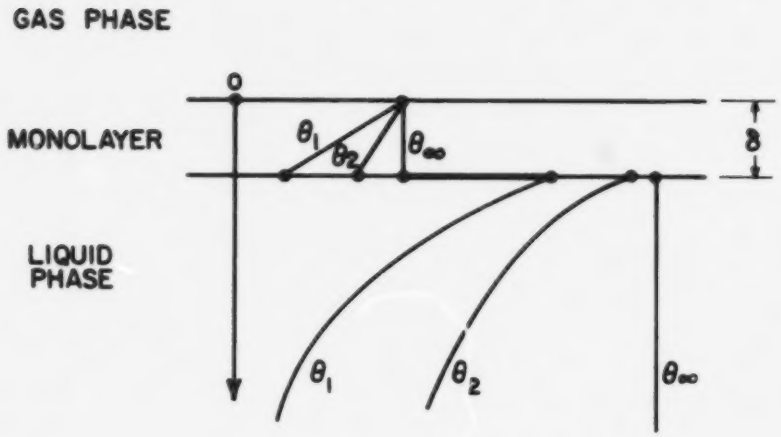

FIGURE 2-2 VARIATION OF CONCENTRATION.

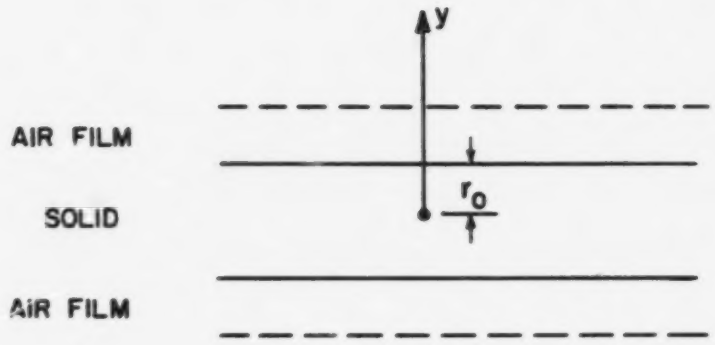

FIGURE 2-3 COORDINATES USED BY ROHSENOW AND CHOI.

where C is the concentration of the carbon dioxide in the water phase and m is the distribution coefficient.

As was introduced earlier, the transport within the water is represented by the equation

$$\frac{\partial C}{\partial \theta} = D_w \frac{\partial^2 C}{\partial y^2} \qquad (2\text{-}45)$$

with the following boundary conditions

$$C\ (0,y) = C_i \qquad (2\text{-}46)$$

$$\frac{\partial C}{\partial y}\ (\theta,0) = 0 \qquad (2\text{-}47)$$

$$- D_w \frac{\partial C}{\partial y}\ (\theta,h) = k\Delta\overline{C} = N \qquad (2\text{-}48)$$

where $\Delta\overline{C}$ is the concentration gradient across the monolayer.

This solution uses the same reflection principle as that used in the clean surface case. That is, we are only interested in the upper half of the problem as shown in Figure 2-3. The bottom reflection is assumed for mathematical convenience. Boundary condition (2-46) states that initially there is no carbon dioxide in the water. Boundary condition (2-47) represents a flat profile at the center, and boundary condition (2-48) assumes steady state mass transfer across the monolayer. If equilibrium is assumed at both surfaces of the layer, we may eliminate the gas concentration within the layer and write

$$\Delta\overline{C} = \frac{P}{H} - C\ (\theta,h) \quad . \qquad (2\text{-}49)$$

In the present case the gas was always pure and at

atmospheric pressure, therefore;

$$\Delta\overline{C} = \left[\frac{1}{H} - \frac{C}{m} (\theta,h) \right] \quad . \tag{2-50}$$

Making the following translation of the concentration variable

$$P (\theta,y) = \left[C (\theta,y) - \frac{m}{H} \right] \tag{2-51}$$

the problem becomes

$$\frac{\partial P}{\partial \theta} = D_w \frac{\partial^2 P}{\partial y^2} \tag{2-52}$$

with boundary conditions

$$P (0,y) = - \frac{m}{H} \tag{2-53}$$

$$\frac{\partial P}{\partial y} (\theta,0) = 0 \tag{2-54a}$$

$$\frac{\partial P}{\partial y} (\theta,h) = - \frac{k}{mD_w} P (\theta,h) \quad . \tag{2-54b}$$

Then setting

$$P_i = - \frac{m}{H} \tag{2-55}$$

$$N = - \frac{k}{mD_w} \quad , \tag{2-56}$$

and

$$h = r_o \quad , \tag{2-57}$$

the boundary conditions have been restated as

$$P (0,y) = P_i \tag{2-58}$$

$$\frac{\partial P}{\partial y} (\theta,0) = 0 \tag{2-59}$$

$$\frac{\partial P}{\partial y}(\theta, r_o) = - N P (r_o, \theta) \quad . \qquad (2\text{-}60)$$

Equations (2-52), (2-58), (2-59), and (2-60) state the problem exactly as presented in Rohsenow and Chow (37), for which the solution is

$$\frac{P}{P_i} = 2 \sum_{n=1}^{\infty} \left[\frac{\sin \lambda_n r_o}{\lambda_n r_o + \sin \lambda_n r_o \cos \lambda_n r_o} \right] e^{-\lambda_n^2 D_w \theta} \cdot \cos \lambda_n y \qquad (2\text{-}61)$$

where λ_n's are given by the solution to

$$\cot \lambda_n r_o = \frac{1}{N r_o} (\lambda_n r_o) \quad . \qquad (2\text{-}62)$$

The average concentration in the liquid at any time is

$$\langle C \rangle = \frac{1}{r_o} \int_0^{r_o} C \, dy \quad . \qquad (2\text{-}63)$$

This may be expressed in terms of P as follows

$$\frac{P}{P_i} = \frac{C - \frac{m}{H}}{-\frac{m}{H}} = \left[1 - \frac{HC}{m} \right] \quad , \qquad (2\text{-}64)$$

as

$$C = \frac{m}{H} \left[1 - \frac{P}{P_i} \right] \quad , \qquad (2\text{-}65)$$

then

$$\langle C \rangle = \frac{m}{H} \left[1 - \frac{1}{r_o} \int_0^{r_o} \frac{P}{P_i} \, dy \right] \quad . \qquad (2\text{-}66)$$

Now, employing the solution to obtain

$$\frac{1}{h} \int_0^h \frac{P}{P_i} \, dy = 2 \sum_{n=0}^{\infty} \left[\frac{\sin \lambda_n r_o}{\lambda_n r_o + \sin \lambda_n r_o \cos \lambda_n r_o} \right] e^{-\lambda_n^2 D_w \theta} \frac{1}{r_o} \int_0^{r_o} \cos \lambda_n y \, dy \quad , \qquad (2\text{-}67)$$

integration leads to

$$C = \frac{m}{H}\left[1 - 2\sum_{n=0}^{\infty} \frac{\left[\sin\left(\lambda_n r_o\right)\right]^2 e^{-\lambda_n^2 D_w \theta}}{\lambda_n r_o\left[\lambda_n r_o + \sin\lambda_n r_o \cos\lambda_n r_o\right]}\right] . \quad (2\text{-}68)$$

The amount of gas in the water at any time is

$$\Delta n = V_1 \langle C \rangle \quad (2\text{-}69)$$

and combining, then

$$\frac{H}{m}\frac{\Delta n}{V_1} = \left[1 - 2\sum_{n=0}^{\infty} \frac{\left[\sin\left(\lambda_n r_o\right)\right]^2 e^{-\lambda_n^2 D_w \theta}}{\lambda_n r_o\left[\lambda_n r_o + \sin\lambda_n r_o \cos\lambda_n r_o\right]}\right] . \quad (2\text{-}70)$$

The percent of unsaturation, or one minus the saturation value from (2-70), gives

$$\left[1 - \frac{H}{m}\frac{\Delta n}{V_1}\right] = 2\sum_{n=0}^{\infty} \frac{\left[\sin\left(\lambda_n r_o\right)\right]^2 e^{-\lambda_n^2 D_w \theta}}{\lambda_n r_o\left[\lambda_n r_o + \sin\lambda_n r_o \cos\lambda_n r_o\right]} . \quad (2\text{-}71)$$

From equations (2-43) and (2-44) it is noted that m/H is the water concentration at the layer-water interface. If

$$C_i = \frac{m}{H} \quad (2\text{-}72)$$

where C_i is the solubility of gas in water when they are in direct contact, it is assuming that the water surface becomes saturated as if the monolayer were not present. The layer still plays an important role in the rate of absorption. For this reason, we use a carbon dioxide-water saturation value for m/H.

Then

$$\left[1 - \frac{\Delta n}{C_i V_1}\right] = 2\left\{\frac{\left[\sin\left(\lambda_1 r_o\right)\right]^2 e^{-\lambda_1^2 D_w \theta}}{\lambda_1 r_o\left[\lambda_1 r_o + \sin\lambda_1 r_o \cos\lambda_1 r_o\right]} + \right.$$

$$\left. \frac{\left[\sin\left(\lambda_2 r_o\right)\right]^2 e^{-\lambda_2^2 D_w \theta}}{\lambda_2 r_o\left[\lambda_2 r_o + \sin\lambda_2 r_o \cos\lambda_2 r_o\right]} + \cdots \right\} \quad . \qquad (2\text{-}73a)$$

Assuming that only the first term of the series is required for times greater than 2000 seconds, because of the success of the previous model, (2-73b) is obtained,

$$\left[1 - \frac{\Delta n}{C_i V_1}\right] = \frac{2\left(\sin\lambda_1 r_o\right)^2 e^{-\lambda_1^2 D_w \theta}}{\lambda_1 r_o\left[\lambda_1 r_o + \sin\lambda_1 r_o \cos\lambda_1 r_o\right]} \quad . \qquad (2\text{-}73b)$$

Taking the logarithim of (2-73b), (2-74) is then obtained.

$$\ln\left[1 - \frac{\Delta n}{C_i V_1}\right] = \ln\left[\frac{2\left(\sin\lambda_1 r_o\right)^2}{\lambda_1 r_o\left[\lambda_1 r_o + \sin\lambda_1 r_o \cos\lambda_1 r_o\right]}\right]$$

$$-\lambda_1^2 D_w \theta \quad . \qquad (2\text{-}74)$$

A plot of $\left[1 - \frac{\Delta n}{C_i V_1}\right]$ versus time will give a straight line with a slope of $-\lambda_1^2 D_w$.

Evaluating $-\lambda_1^2 D_w$ from equation (2-74), λ_1 is given by

$$\cot \lambda_1 r_o = \left[\frac{m D_w \lambda_1}{k}\right] \quad , \qquad (2\text{-}75)$$

where r_o is the depth of the water.

Goodridge and Robb (17) reported an experimental value of 2.07×10^{-3} cm/sec for the mass transfer coefficient for a monolayer of n-hexadecanol. Their experiment was similar to the present one in that the rate of carbon dioxide absorption into water was measured. However, they employed a stirred tank where the present study uses a ripple tank. The authors (17) avoided the need for the solubility of carbon dioxide in n-hexadecanol by using an overall mass transfer coefficient.

Value of the Bunsen absorption coefficient, α, (24) for some chemicals similar to n-hexadecanol are given in Table A-S1. As can be seen from this table, it is reasonable to assume a Bunsen coefficient of approximately 1.5 for n-hexadecanol. From Equation (2-43) the saturation concentration of carbon dioxide in n-hexadecanol for a partial pressure of one atmosphere is

$$C = \frac{\alpha}{24{,}000.} = \frac{1.5}{24{,}000.} = 6.7 \times 10^{-5} \text{ gmoles/ml} \quad .$$

The corresponding value of the Henry's law constant at 25°C is

$$H = 22{,}400./1.5 = 1.5 \times 10^{4} \text{ atm ml/gmole} \quad .$$

The distribution coefficient of carbon dioxide between n-hexadecanol and water is given by Equation (2-44). From Figure B-2, $C_i = 3.42 \times 10^{-5}$, and from the above considerations $C = 6.7 \times 10^{-5}$ gmoles/ml. Thus the distribution

coefficient at 25°C is

$$m = 3.42 \times 10^{-5}/6.7 \times 10^{-5} = 0.51 \quad .$$

The above values of m and k were used in calculating the value of D_w for the monolayer model.

Letting the slope be the magnitude of Equation (2-74) we can write the following two equations

$$[S1] = \lambda_1^2 D_w \tag{2-76}$$

and

$$\cot\left(\lambda_1 r_o\right) = -\frac{m}{k} D_w \lambda_1 \tag{2-77}$$

and eliminating λ_1 between (2-76) and (2-77) where $r_o = h$, yields

$$\cot\left[h\sqrt{\frac{S1}{D_w}}\right] = -\frac{m}{k}\sqrt{S1 \times D_w} \quad . \tag{2-78}$$

After the value of the slope for a run had been determined, Equation (2-78) was solved by trial and error for D_w.

The above values of m and k are open to some question. Goodridge and Robb (17) estimated a value of k from absolute reaction rate theory that was 10^{-27} times their experimental value. As can be seen from Equation (2-78), the values of D_w are bounded by two limits.

The lower limit occurs when

$$\frac{m}{k}\sqrt{S1\ D_w} \to 0 \quad , \tag{2-79}$$

so

$$h\sqrt{\frac{Sl}{D_w}} = \frac{\pi}{2} \quad , \tag{2-80}$$

or

$$D_w = \frac{4h^2 Sl}{\pi^2} \quad . \tag{2-81}$$

This is what would happen if no monolayer were present. Thus the monolayer model is more general and includes the clean surface model of Muenz (34) as a special case.

The other limit occurs when in Equation (2-78)

$$\frac{m}{k}\sqrt{Sl\ D_w} \to \infty \quad , \tag{2-82}$$

Then (15)

$$\cot\left[h\sqrt{\frac{Sl}{D_w}}\right] = -\infty \quad , \tag{2-83}$$

so

$$h\sqrt{\frac{Sl}{D_w}} = \pi \quad , \tag{2-84}$$

or

$$D_w = \frac{h^2 Sl}{\pi} \quad . \tag{2-85}$$

This limit gives D_w values that are one-fourth of the previous limit.

In processing this data for the latter limit, again a two point procedure can be used for the slope, or

$$\ln\left[\frac{\left(1 - \frac{\Delta n}{C_i V_l}\right)_1}{\left(1 - \frac{\Delta n}{C_i V_l}\right)_2}\right] = Sl\left(\theta_2 - \theta_1\right) \tag{2-86}$$

where slope = $Sl = -\lambda_1 D_w$.

CHAPTER III

MASS TRANSFER EXPERIMENTS

General

This chapter describes the equipment and the procedure employed in obtaining data for the determination of the rate of absorption of carbon dioxide into water. A small ripple tank was used for these studies. The data presented in subsequent chapters was obtained by methods similar to those described in this section.

The direction of mass transfer was always from the gas phase to the liquid phase. The carbon dioxide used was of commercial grade, containing less than one percent impurities, and was used as received. The carbon dioxide was saturated by bubbling it through distilled water to eliminate any interphase water transfer. The water used in the absorption studies was distilled and deaerated to eliminate any impurities that might affect the overall transfer.

The total gas absorbed by the water was measured as a function of time in the unsteady state non-flow system. Experiments were made with a clean surface, no monolayer, where the parameters studied were liquid depth and wave frequency. Also experiments were performed to study the effect of a surface active agent, n-hexadecanol, on mass transfer. In this case the amount of n-hexadecanol solution and wave frequency were the parameters. Wave frequencies of 400, 600,

and 800 cycles per minute were used in this dissertation to be consistent with the data obtained by Muenz (34).

Procedure

Deaeration of Water: For all mass transfer runs, it was necessary to produce deaerated water before a run could begin. Distilled water from the laboratory tap filled the system shown schematically in Figure 3-1. The system consisted of a heating apparatus which was a two gallon stainless steel container in which immersion heaters were placed. A two gallon reservoir blanketed by a heat exchanger was in line to contain the final deaerated water. Connecting these with the ripple tank was a circulation system using a series of ball valves and a circulating pump. The circulation rate was one to two gallons per minute. The overall system is shown in Figure 3-2.

For deaeration, the heaters were switched on and their voltage was controlled by a Variac. After the water in the heating vessel has started to boil, the circulation system was started with all valves open except the tank valve and the vent valve. After one hour of circulation heating, the water was at a boil. The Variac was adjusted to maintain a slow boil for the next hour, after which, the system was shut down by first stopping the pump, then closing the valve at the pump exit and the valve from the storage vessel to the heating vessel, thus giving a trapped system of deaerated water in the reservoir. The water was allowed to cool

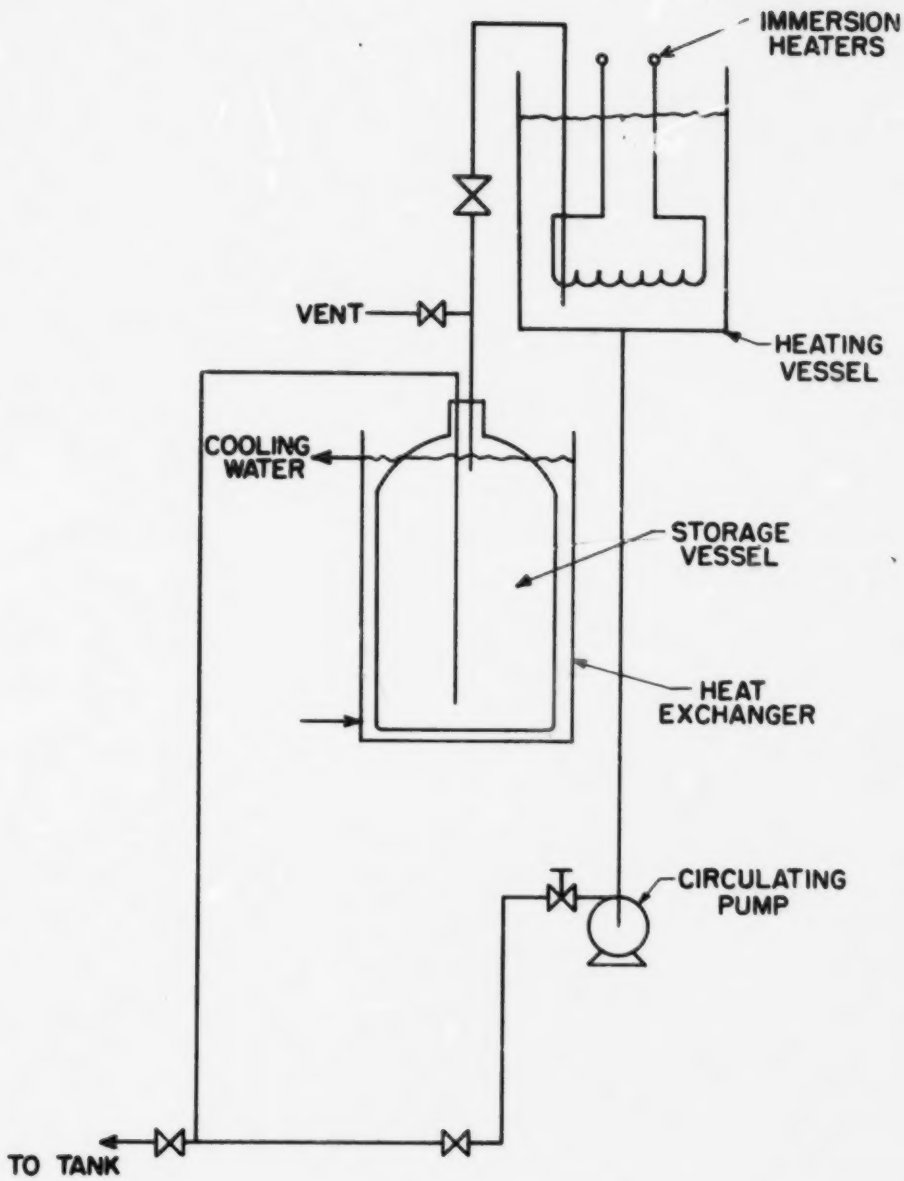

FIGURE 3-1 WATER DEAERATION APPARATUS

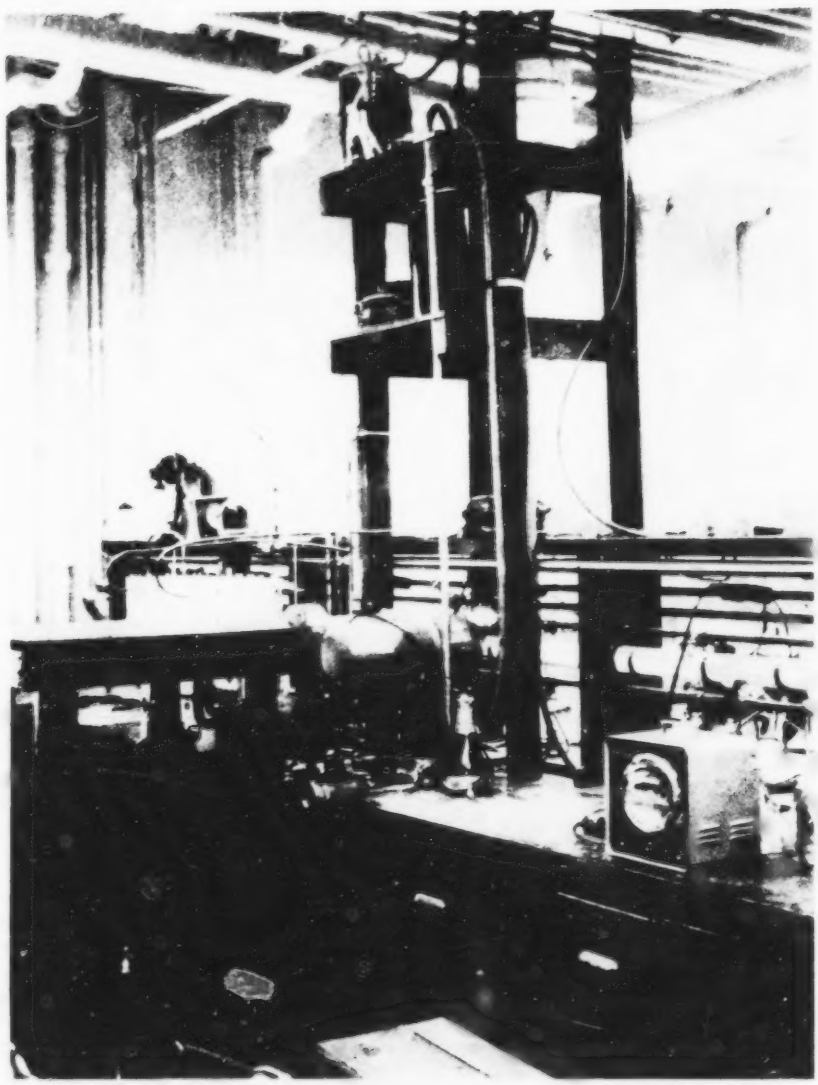

FIGURE 3-2 PHOTOGRAPH OF OVERALL APPARATUS.

overnight, and before use it was cooled slightly below room temperature to prevent condensation on the tank walls. Such condensation would cause an undesirable increase in transfer area. This procedure was repeated before each run.

Purging the Tank: After producing a reservoir of deaerated water, the previously dried ripple tank was purged with saturated carbon dioxide for two hours before each run. As shown in Figure 3-3 the carbon dioxide is regulated directly from a commercial cylinder through a glass scintered sparger immersed in distilled water. Saturation was checked by measuring the wet bulb temperature. In all cases no temperature drop was recorded, whereas the same test using carbon dioxide from the cylinder produced a twenty degree temperature drop.

Carbon dioxide entered the tank at a rate of 0.05 SCFM. Initially all vents and drain lines to the tank were left open. The top vent was closed forcing the purging gas through the tank as well as the wave generation portion of it. This was done to assure complete removal of all impure substances. After an hour the top vent was reopened and the drain valve closed for final purging. After a two hour purge, the gas flow was stopped and all vents closed, thus trapping saturated carbon dioxide within the tank. During this purging process, the containment flask for use in volume adjustment was also purged and sealed for each run. The system was then prepared for a mass transfer run.

The Mass Transfer Process: After deaeration of water

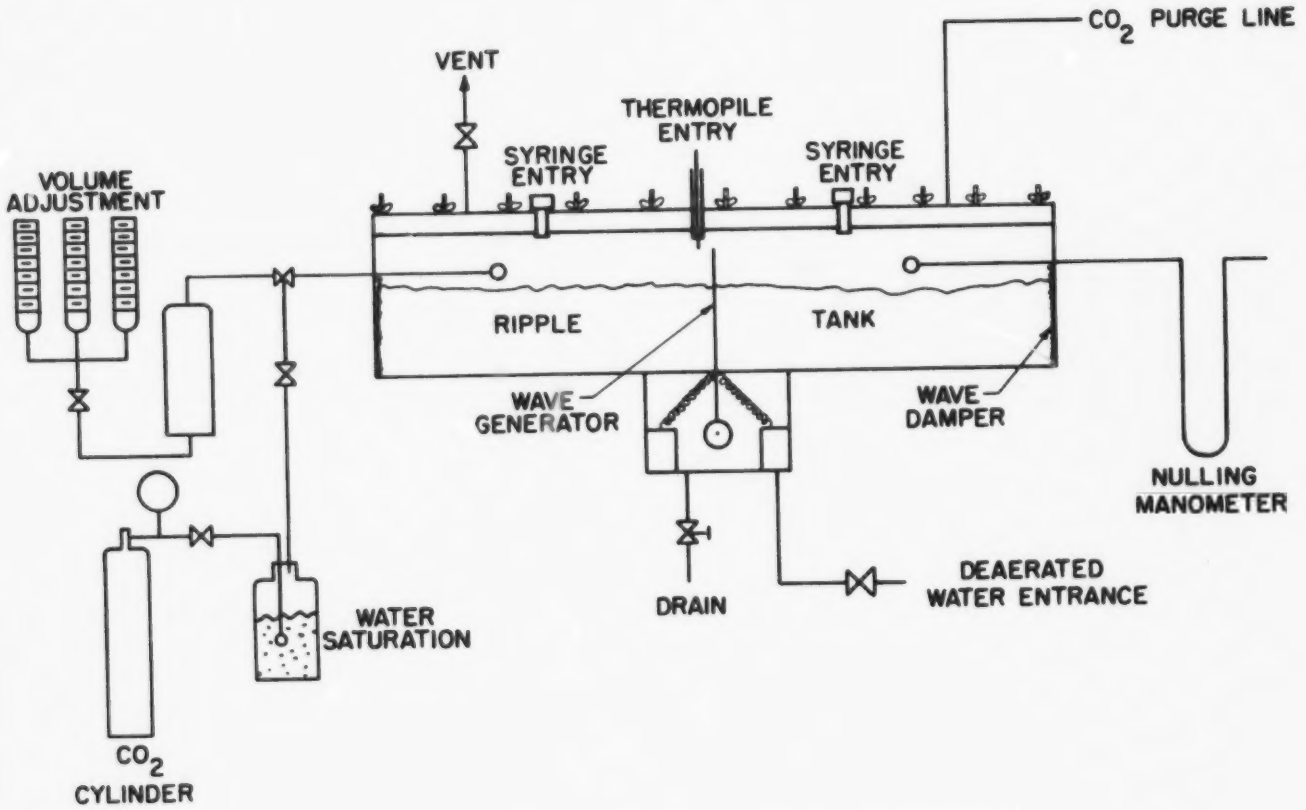

FIGURE 3-3 MASS TRANSFER EQUIPMENT

and purging of the tank with carbon dioxide, a mass transfer run could be made. The tank vent was opened to allow excess trapped gas to exit during water filling. The deaerated water reservoir vent was opened and the valve between the storage vessel and the tank was regulated to allow the correct amount of water to enter the ripple tank. In most runs this amount was a two inch water level, except in the level variation case. After the water entered the tank, the surface active agent, n-hexadecanol, was distributed through two syringe caps on top of the tank in the monolayer case. In this case, after waiting several minutes, the wave generation system was started and the tank vent closed, at which time mass transfer data could be recorded. In the no surface agent case, after the water entered, the wave generation system was immediately started and upon closing the tank vent, mass transfer data taken. The final case of a no wave run involved only the closing of the tank vent and the recording of mass transfer data. The ripple tank in operation is shown in Figure 3-4.

The recording of this data was accomplished in the following manner. The barometric pressure of the room was recorded, as well as the initial temperature of the tank. As the water entered, its initial temperature was recorded. The wave generator, which had been set previous to the run, was rechecked by a Cenco strobe to be sure of the exact frequency. Upon closing of the tank vent, absorption began immediately. To measure this absorption, carbon dioxide from

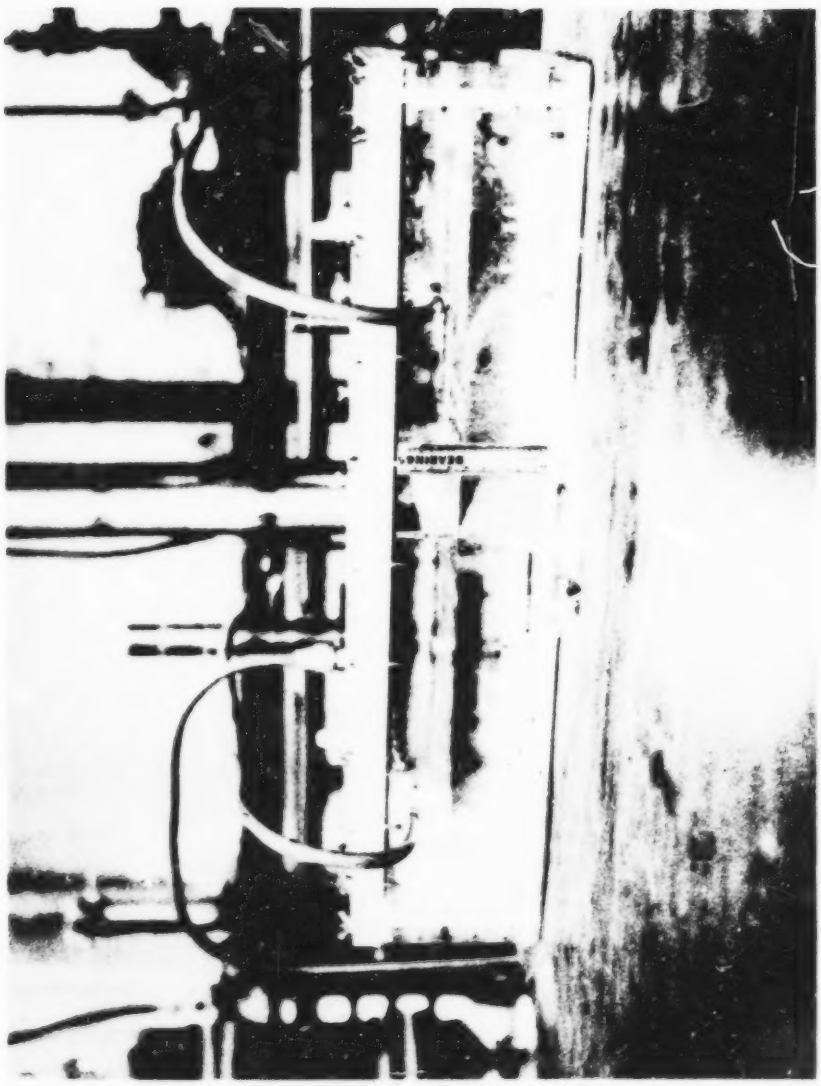

FIGURE 3-4 PHOTOGRAPH OF RIPPLE TANK

the containment flask was regulated by a needle valve to keep the manometer nulled. By this nulling, leaks were minimized with the tank maintained at atmospheric pressure, and an easy method of obtaining PVT data was obtained. By running at atmospheric pressure, no variation in equilibrium saturation gas concentration was obtained. The volumetric measuring device used to accomplish this nulling is shown in Figure 3-5.

At normal increments mass transfer data were recorded. These data were the barometric pressure, the gas temperature, the amount of water necessary to displace the gas in the containment flask, and the total time elapsed. After periodically recording these data for two hours, the system was shut down and the final water temperature taken. If the next run were to be of a different frequency, this frequency was set with the strobe. Water in the ripple tank was then drained and the tank purged with compressed air until it was completely dry.

Equipment

Water Deaeration Apparatus: As shown in Figure 3-1, the immersion heaters were of the coil type having a total output of 2250 watts on 110 volts of AC power. The heating vessel was a two gallon stainless steel beaker wrapped in asbestos insulation to prevent dissipation of heat. The storage vessel was a two and one-half gallon glass stoppered bottle wrapped in masking tape. This held the deaerated water until the mass transfer experiment was run. The heat exchanger was a five gallon container fitted with inlet and

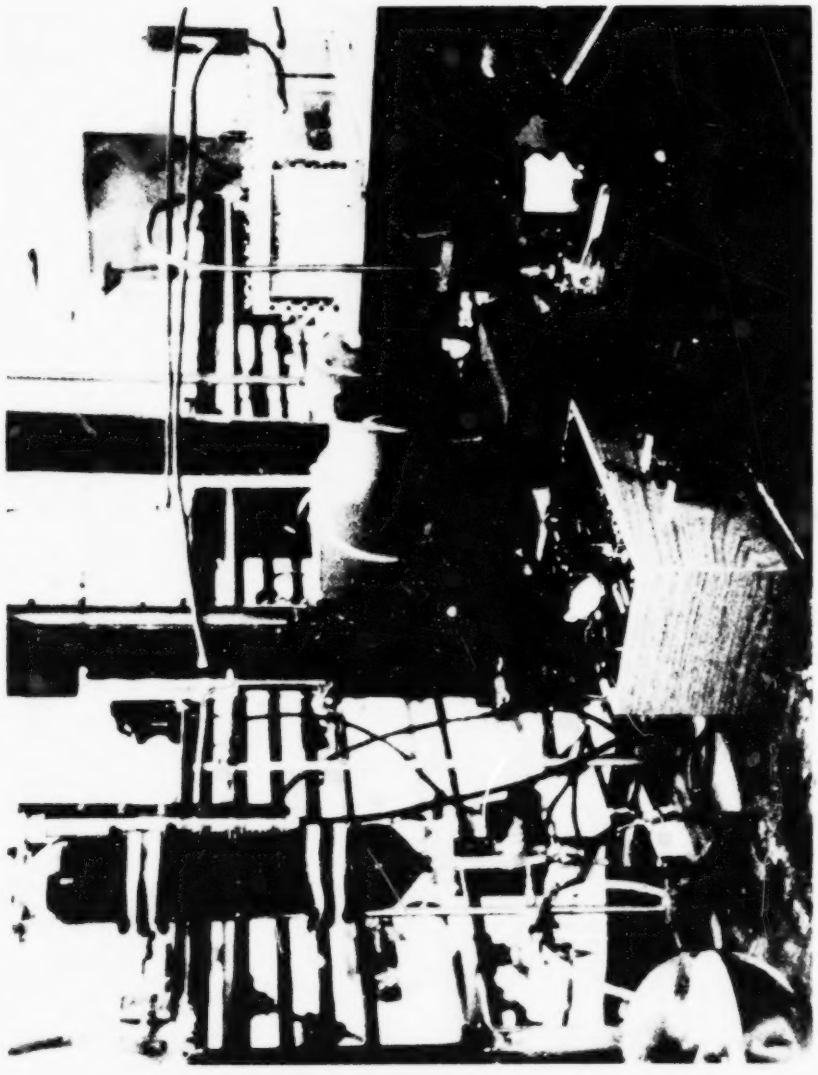

FIGURE 3-5 PHOTOGRAPH OF VOLUMETRIC APPARATUS.

outlet cooling water spouts. The circulation pump was an Eastern type 80010 with a seven gallon per minute capacity. As shown in Figure 3-1, four ball valves and one globe valve were used to complete the circulation system.

Mass Transfer Equipment: The ripple tank shown in Figure 3-3 was constructed of 3/4" plexiglass. With dimensions of 20" by 6" by 4" deep it was fitted with a wave generation compartment below the mass transfer space. The wave generation system was separated from the transfer compartment by a plexiglass partition with a slot to allow the rods to travel freely. The generation system itself consisted of 25 rigidly supported vertical stainless steel rods 0.053 inches in diameter spaced 1/4" apart. The system was placed in the center of the tank to produce symmetric conditions throughout. The rods moved up and down in notched groves in the tank sides. They were driven by a variable speed motor through a spring loaded camshaft of 1/4" lift. This up and down motion of the assembly caused each rod to produce a circular wave. These circular waves upon joining traveled down the tank as a two dimensional wave front. Upon intercepting the end of the tank, wire screening enwrapped in gauze damped them thus preventing reflection. The wave generation system was also equipped with a small lift cam, however, it was not used in this analysis.

The tank was sealed by an "O" ring recessed in a 1/16" groove on the lip of the tank. A 3/4" plexiglass top was then fastened to the tank lip by a series of evenly

spaced taps fitted with wingnuts, which when drawn tight against the "O" ring produced an excellent seal. The top was fitted with a thermopile entry into which a five lead thermocouple of copper-constantine was run. Two entry ports for a hypodermic syringe which applied the n-hexadecanol were also fitted to the top of the tank. The tank was vented using a 1/4" copper line and a ball valve. A U-tube manometer with one leg open to the atmosphere, and a carbon dioxide entry port were attached to the side of the tank.

Deaerated water entered the tank through the wave generation chamber, and after use it was expelled through a drain in the chamber. The volume adjustment apparatus consisted of a 2250 ml containment flask which held the saturated carbon dioxide used for absorption. Connected in series with the containment flask were three 300 ml measuring buretts which held water used to displace the carbon dioxide from the containment flask. The rate of displacement was controlled by a small needle valve between the measuring buretts and the containment flask.

The carbon dioxide was saturated with water by passing it through a scintered glass sparger at a relatively slow flow rate. The nulling manometer was a U twenty inch vertical type. The cam was driven by a Reeves Drive variable speed motor of one half horsepower which produced controlled speeds of 300 to 1200 rpm. A five lead thermopile of copper-constantine was used to measure the gas temperature. A Brown "precision" potentiometer capable of reading to 0.001 millivolts was

used to measure the emf produced by the thermopile.

Presentation of Data

The data obtained in this investigation are presented in Appendix A in Tables A-1 through A-M4. The data is presented as total moles of absorbed carbon dioxide versus time. These data were plotted and the slope determined in accordance with the mathematical model, giving an empirical value of the effective diffusivity, which is a combination of the molecular diffusivity and the eddy diffusivity.

It was necessary to correct for any temperature changes during a run by utilizing the ideal gas law in the form:

$$V_c = V_{abs} + V_{gs} \ (1 - T/T_i) \qquad (3\text{-}1)$$

where V_c is the final corrected volume, V_{abs} is the volume of the gas actually measured with respect to time, V_{gs} is that volume measured above the absorbing water, T the temperature of the gas at the time of the reading, and T_i the initial temperature of the gas space as recorded before the mass transfer study progressed.

To determine the volume of the gas space, V_{gs}, in the tank as a function of liquid depth, again the ideal gas law was utilized in the following form:

$$P_1 \ V = P_2 \ (V_{gs} - d) \qquad (3\text{-}2)$$

where P_1 and P_2 are the pressure readings before and after

the addition of a gas to the sealed tank, and d is the measured change in volume. Knowing these, V_{gs}, the volume of the gas space could be calculated for that particular depth. Figure B-1 in Appendix B represents a curve of the gas space volume as a function of liquid depth.

In order to determine the effect of the gauze dampers on mass transfer, a run was made without this damping device. This zero wave run was compared to the zero wave run with the gauze. The order of magnitude analysis of the error was less than five percent thus its contributive error was neglected.

CHAPTER IV

ANALYSIS AND DISCUSSION

Data Analysis

The raw data for each run are presented in Appendix A, Tables A-1 through A-M4. They are presented as the total moles of carbon dioxide absorbed in the liquid phase versus the time in seconds. These raw data were analyzed to determine an effective diffusivity, D_w.

Before using a sample calculation to show the methods of determining D_w, a few of the errors involved and the factors discovered before calculation could proceed will be discussed. Initialization error, or the error of introducing the water into the tank which displaced the carbon dioxide, causing absorption as soon as the two phases were in contact was considered. The actual recording of this absorption started some twenty seconds later in the depth variation case and a few minutes later in the monolayer case. Because of the agreement of the data obtained in this analysis and the fact that runs lasted longer than one hour, it was found that an extrapolation would in most cases be to one on a plot of $(1 - \Delta n/C_i V_l)$ versus time, hence this initialization error could be conveniently neglected.

Another factor considered was the turbulence of the water as it was introduced into the tank. Through experimentation the most efficient method of introducing water to

avoid violent turbulence was found by appropriate regulation of the ball valve in the circulation line. This turbulence was the same for all runs and no attempt was made to account for its error contribution. These disturbances appeared to die out within the first few minutes of the run.

Due to the cooling of the water before it entered the tank, the gas and liquid were not initially at the same temperature, and a short time was required to produce thermal equilibrium. This caused some problems as the utilization of the ideal gas law in the PVT calculation was subjected to these temperature changes. As explained in Chapter III, this cooling was necessary to eliminate condensation on the tank walls thus eliminating an increase in absorption area. Equation (3-1) was used in this correction,

$$V_c = V_{abs} + V_{gs} \ (1 - T_i/T)$$

where V_{gs}, the volume of the gas space above the tank was determined quantatively and is presented as a function of liquid depth in Appendix B, Figure B-1. The temperature change caused by the contact of the cooler water with the warmer gas was usually no more than a few degrees.

The temperature change of the gas phase also introduced variation in the temperature sensitive equilibrium constant values, or C_i values. Rather than determine an average temperature for each run, the actual concentration at a particular temperature of a reading was used in the calculation. The value itself was taken from Figure B-2 in

Appendix B, which plots the equilibrium constant, C_i, versus the temperature in degrees centigrade. These data were obtained from the International Critical Tables (24) in the form of a Henry's law constant.

After the above corrections had been made and recorded, the actual reduction of data was begun. From the total moles absorbed versus time data, and the equilibrium constant versus temperature, and the knowledge of the volume of liquid in the tank at each particular liquid depth, the percent of saturation could be calculated. The fractional attainment of saturation was represented by $\Delta n/C_i V_l$ where Δn is the total moles of carbon dioxide absorbed, C_i is the equilibrium constant corrected to a particular temperature, and V_l is the volume of the water in the tank. Since this represents the degree of saturation, $(1 - \Delta n/C_i V_l)$ represents the degree of unsaturation. These data are then plotted on semilog paper as $(1 - \Delta n/C_i V_l)$ versus the time in seconds. A sample of this plot is shown in Figure 4-1 for run number A-5. This plot is from the data for the no monolayer, no wave, and no gauze in the tank end case. After inspecting Figure 4-1, and finding that it does present a straight line, a two point slope determination was performed, and the slope used in determining the value of D_w was found.

In the depth variation case or no monolayer case which Figure 4-1 represents, the slope determination and hence the determination of D_w can be represented by the following calculation, based on the discussion in Chapter II.

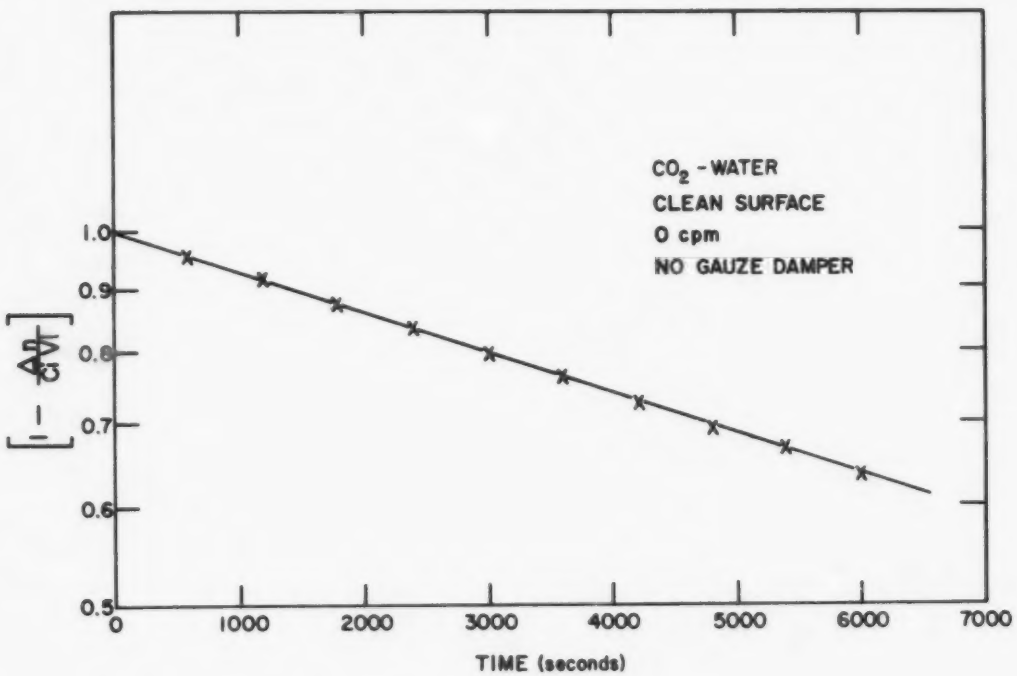

FIGURE 4-1 TYPICAL RAW DATA PLOT

$$\ln \left[1 - \frac{\Delta n}{C_i V_1} \right]_2 = \ln \left[\frac{8}{\pi^2} \right] - \left[\frac{D_w \pi^2 \theta_2}{4h^2} \right] \qquad (4\text{-}1)$$

is added to

$$- \ln \left[1 - \frac{\Delta n}{C_i V_1} \right]_1 = - \ln \left[\frac{8}{\pi^2} \right] + \left[\frac{D_w \pi^2 \theta_1}{4h^2} \right] \qquad (4\text{-}2)$$

and combining within the logarithm yields

$$\ln \left[\frac{\left(1 - \frac{\Delta n}{C_i V_1} \right)_2}{\left(1 - \frac{\Delta n}{C_i V_1} \right)_1} \right] = \frac{D_w \pi^2}{4h^2} \left(\theta_2 - \theta_1 \right) \quad . \qquad (4\text{-}3)$$

The actual calculation is as follows. The data used are taken from points of Figure 4-1 at 3000 and 6000 seconds. Then

$$\ln \left[\frac{(-.789)}{(-.635)} \right] = \frac{D_w \pi^2}{(4)(5.08)^2} (6000 - 3000) \qquad (4\text{-}4)$$

and D_w then equals 7.96×10^{-4} cm^2/sec.

In the monolayer case the same corrections are involved before calculation as in the depth variation study. The initialization error is greater because of the time necessary to produce the monolayer. However, this error can be neglected, as in most cases extrapolation of the $(1 - \Delta n/C_i V_1)$ versus time curve leads to one. Temperature corrections are made in a like manner and the percent of unsaturation is plotted versus the time in seconds. Using the mathematical model below, the slope is obtained

$$\ln \left[\frac{\left(1 - \frac{\Delta n}{C_i V_1}\right)_2}{\left(1 - \frac{\Delta n}{C_i V_1}\right)_1} \right] = Sl \left(\theta_2 - \theta_1\right) \qquad (4\text{-}5)$$

The value of D_w was then obtained by solving the relation

$$\cot \left[h\sqrt{\frac{Sl}{D_w}} \right] = - \frac{m}{k} \sqrt{Sl \times D_w} \quad , \qquad (2\text{-}78)$$

where $k = 2.07 \times 10^{-3}$ cm/sec, and $m = 0.51$. These values were discussed earlier in Chapter II. In addition it was pointed out that the D_w values are bounded by the limits of the above equation. The resulting D_w values may differ by a factor of 4. That is, if no monolayer were assumed to be present, one would obtain a certain value for D_w. On the other hand if the resistance of the monolayer is very large, the resultant D_w for the same data would be one-fourth this value. The actual case lies somewhere in between.

Discussion

Clean Surface Depth Variation Case: By the methods discussed in the preceeding section, values of D_w were determined for a clean surface wave and no wave cases at various liquid depths. These data are represented as a function of depth in Figure 4-2. The depths used in this analysis were 5.08, 2.54, 1.27, and 0.635 centimeters. Data were taken for a no wave case as well as for waves produced at 400, 600, and 800 cycles per minute. Figure B-3 in Appendix B represents the theoretical relation for wavelength versus frequency at

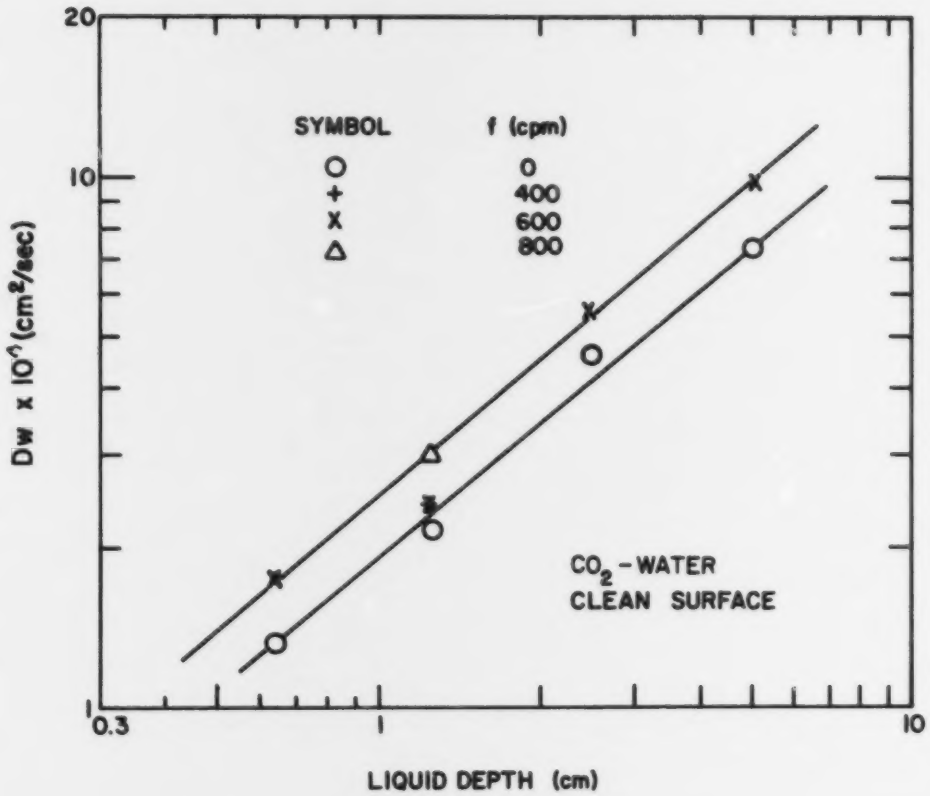

FIGURE 4-2 VARIATION OF EFFECTIVE DIFFUSIVITY WITH DEPTH

various liquid depths. These frequencies were produced by a variable speed motor setting as represented in Figure B-4 of Appendix B.

The values for the effective diffusivity are listed in Table 4-1. When compared singularly with the value of molecular diffusivity, 2.0×10^{-5} cm^2/sec, they are greater than five times that value. This supports the argument for movement in the liquid phase, as for the value to be that of molecular diffusion, the liquid phase must remain motionless. The possibility of background vibrations producing this motion is discounted because of the reproducibility of the data, particularly the no wave runs. The liquid motion which results is due to natural convection and causes higher mass transfer rates.

Natural convection arises from one of two phenomena, either a buoyant effect related to changing fluid densities during heat or mass transfer, or that due to an act of solution, as well as the temperature effect of the heat of solution on the surface tension. The most familiar effects occur in fluids exposed to heated or cooled fixed surfaces. In gas absorption the effect of temperature in the heat of solution can be calculated by a simple heat balance.

Heat Balance: The system is adiabatic in that very little heat is transferred to the plexiglass or the room, thus all the heat of solution remains in the fluid. Thus it can be written

$$\rho C_p V_l (T_f - T_o) + V_l C_i \Delta H_s = 0 \quad , \qquad (4\text{-}6)$$

TABLE 4-1

VALUES FOR $D_w \times 10^4$

Clean Surface Case

cpm	0	400	600	800
5.08 cm	7.28		9.97	
2.54 cm	4.68		5.52	
1.27 cm	2.18	2.44	2.46	3.03
0.635 cm	1.31		1.71	

or

$$\rho C_p (T_f - T_o) + C_i \Delta H_s = 0 \quad , \qquad (4\text{-}7)$$

where ρ is the density of the solution, C_p the specific heat, T_f the final temperature, T_o the reference temperature, C_i the equilibrium constant, and ΔH_s the heat of solution of carbon dioxide in cal/gmole, then from (4-7), $(T_f - T_o)$ equals 0.171 °C. The value of C_i is taken from Figure B-2 in Appendix B and ΔH_s is taken from reference (24). From this calculation it can be seen that the heat of solution causes a negligible rise in the temperature of the tank.

Since the heat of solution adds very little to the fluid temperature and its motion, an explanation discussed in Sternling and Scriven (42) describing a Marangoni instability may apply. The surface motion arising from this instability is caused by perturbations in surface concentrations, which in turn cause changes in surface tension. Associated with the Marangoni instability are roll cell motions in the body of the fluid. This instability is usually discussed in the study of liquid-liquid systems rather than gas-liquid systems, where the magnitude of its effect is relatively unknown. In summary, three types of flow mechanisms may effect the value of D_w. These are random turbulence along particle paths, drift flow due to the waves, and natural convection related to buoyant or Marangoni effects.

As seen from Table 4-1 the effects referred to in the preceeding paragraph cause the no wave D_w values to be much

higher than the molecular diffusivity. The value for D_w was 1.31×10^{-4} for 0.635 cm liquid depth and increased linearly to a value of 7.28×10^{-4} for a depth of 5.08 centimeters. However, when the values for D_w are determined for driven runs they increase in all cases but only on the order of a few percent over the corresponding no wave values. This phenomena is attributed to the fact that surface waves tend to dampen the natural convection contributions, thus only increasing slightly the value of D_w. Table 4-1 and Figure 4-2 show the quantitative data obtained at the various liquid depths for a carbon dioxide-water system. A slope of 0.825 was obtained for Figure 4-2.

Figure 4-3 is a plot of D_w versus the liquid height squared times the frequency. This plot represents a full range of points used in the height variation analysis for the carbon dioxide-water system. Also included in the plot are the data obtained by Muenz (34). He did not vary the liquid height and thus introduced h^2 for dimensional purposes only. The value of the slope of Figure 4-3 is 0.375 whereas Muenz obtained a value of 0.33 for his range of data.

The increase in surface area due to the wave motion of the surface of the liquid is a contributive factor in the increase of the values of D_w; however, this area increase is small, for the waves studied had amplitude to wavelength ratios less than 0.01 as determined by Muenz.

There is a possibility that as the depth decreased the ellipse of fluid particles at the wave surface flattened

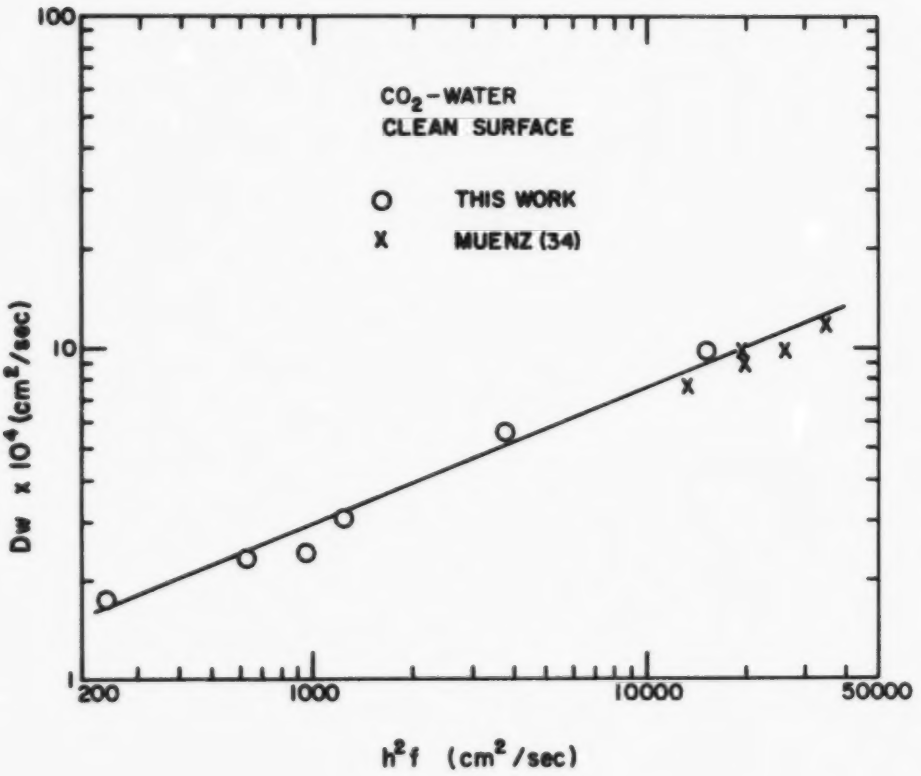

FIGURE 4-3 EFFECT OF LIQUID DEPTH AND WAVE FREQUENCY ON DIFFUSION COEFFICIENT

and the rate of its circulation was decreased, thus decreasing the inherent effective diffusivity. This effect of depth is quite important as shown in Figure 4-2. Large scale circulation or drift would also be greatly reduced by decreasing the liquid depth.

Monomolecular Film Case: To determine the effect of a monolayer on the surface of the liquid phase, both with waves and without, an ethanol solution of n-hexadecanol was prepared. The ethanol aids in the rapid formation of the monolayer by going into solution in the water and depositing the n-hexadecanol on the interface. N-hexadecanol is a solid at room temperature and when placed in the water is much slower in forming the monolayer. Values of D_w were determined with no waves and with waves produced at frequencies of 400, 600, and 800 cycles per minute. The amount of solution necessary for a monolayer varies with frequency. Tables 4-2 and 4-3 represent milliliters of solution used at a particular frequency, and Figures 4-4 and 4-5 show D_w plotted as a function of the volume of solution for a carbon dioxide-water system.

The calculation for the amount of n-hexadecanol necessary for a solution, such that when one milliliter of solution was placed on the still surface, a monolayer would exist, is as follows:

Collision diameter of n-hexadecanol = 4.0×10^{-8} cm

Area of the molecule = $\pi r^2 = 12.56 \times 10^{-16}$ cm^2

Surface area of tank/molecular area = 61.7×10^{16}

then the grams of n-hexadecanol necessary to establish a monolayer equals

$$(A/N_o)\ M = 2.49 \times 10^{-4} \text{ gms} \quad , \qquad (4\text{-}8)$$

where N_o is Avogadros number, and M is the molecular weight of n-hexadecanol. Thus the concentration of the n-hexadecanol solution necessary to establish a monolayer on the liquid phase surface is 0.25 grams/liter. Upon application of one milliliter of this solution, 0.25 grams of n-hexadecanol was distributed on the liquid surface.

The data presented in Table 4-3 and Figure 4-5 are based on the values of k and m given in Chapter II. From this table, it can be seen that the values of D_w increase gradually with the frequency of the waves as in the clean surface case. This would be expected because of the slight increase in surface area or the effects of fluid particle motion. The data plotted in Figures 4-4 and 4-5 show the effect of the n-hexadecanol solution on D_w, and the abrupt breaks in each of the curves represent a transition from a partially covered surface to a completely covered one. In the zero wave case the monolayer appears when about two milliliters of solution are applied to the surface, rather than the calculated one milliliter. The monolayer appears at three milliliters of solution for waves produced at 400 cycles per minute, and at three and one-half for waves produced at a frequency of 600 cycles per minute. A fairly linear curve can be drawn through these three points, and monolayers can be

TABLE 4-2

VALUES OF $D_w \times 10^4$ FOR MONOLAYER

LARGE FILM RESISTANCE

Water Depth = 5.08 cm

ml Solution	Frequency cpm			
	0	400	600	800
0	7.28		9.97	
1/2	2.21			
1	1.47		2.15	
1-1/2	1.28			
1-3/4	0.715			
2	0.406	1.53	1.985	
2-1/2		1.56		
3		1.38	1.94	2.45
3-1/2			1.76	
4		1.34		
4-1/2			1.76	
5	0.216		1.75	

TABLE 4-3

VALUES OF $D_w \times 10^4$ FOR MONOLAYER

SMALL FILM RESISTANCE

ml Solution	Frequency cpm							
	0		400		600		800	
	Slope	D_w	Slope	D_w	Slope	D_w	Slope	D_w
1/2	0.847	8.18						
1	0.562	5.64			.825	7.98		
1-1/2	0.490	4.96						
1-3/4	0.274	2.78						
2	0.156	1.52	0.585	5.75	0.755	7.30		
2-1/2			0.597	5.86				
3			0.528	5.40	0.743	7.12	0.937	8.95
3-1/2					0.675	6.55		
4			0.513	5.10				
4-1/2					0.675	6.55		
5	0.0837	0.882			0.670	6.40		

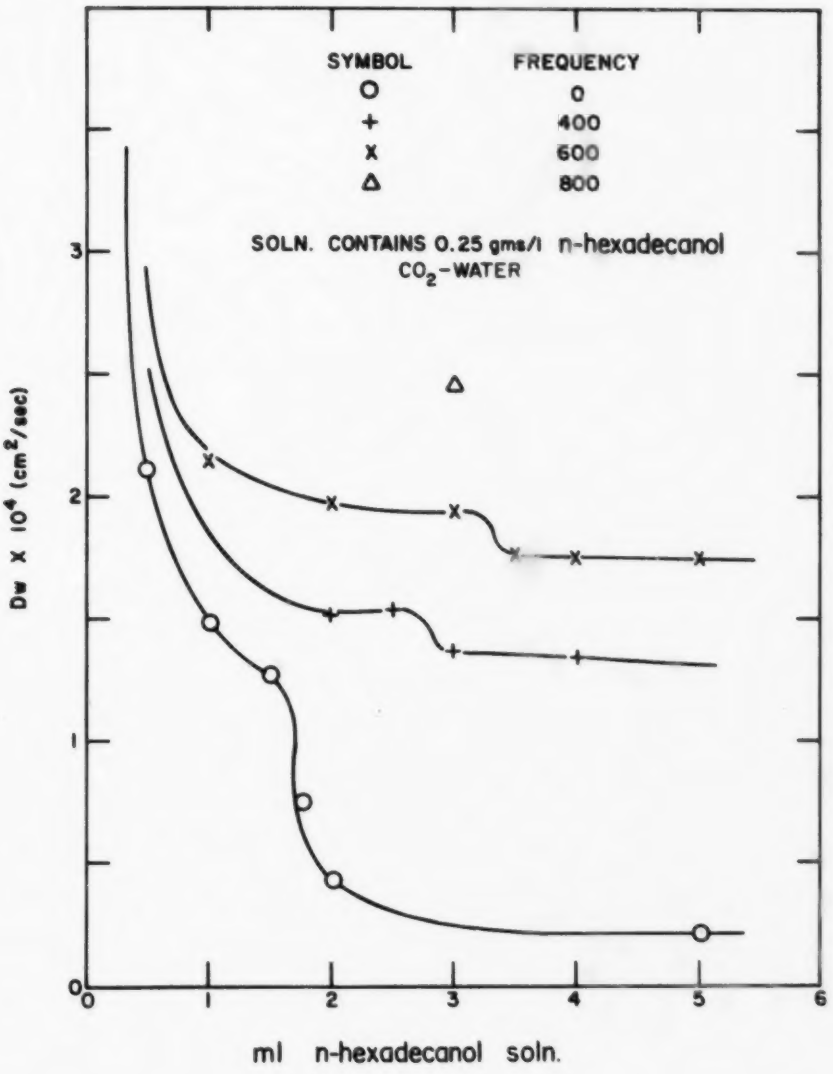

FIGURE 4-4 INFLUENCE OF MONOLAYER ON EFFECTIVE DIFFUSIVITY
LARGE FILM RESISTANCE

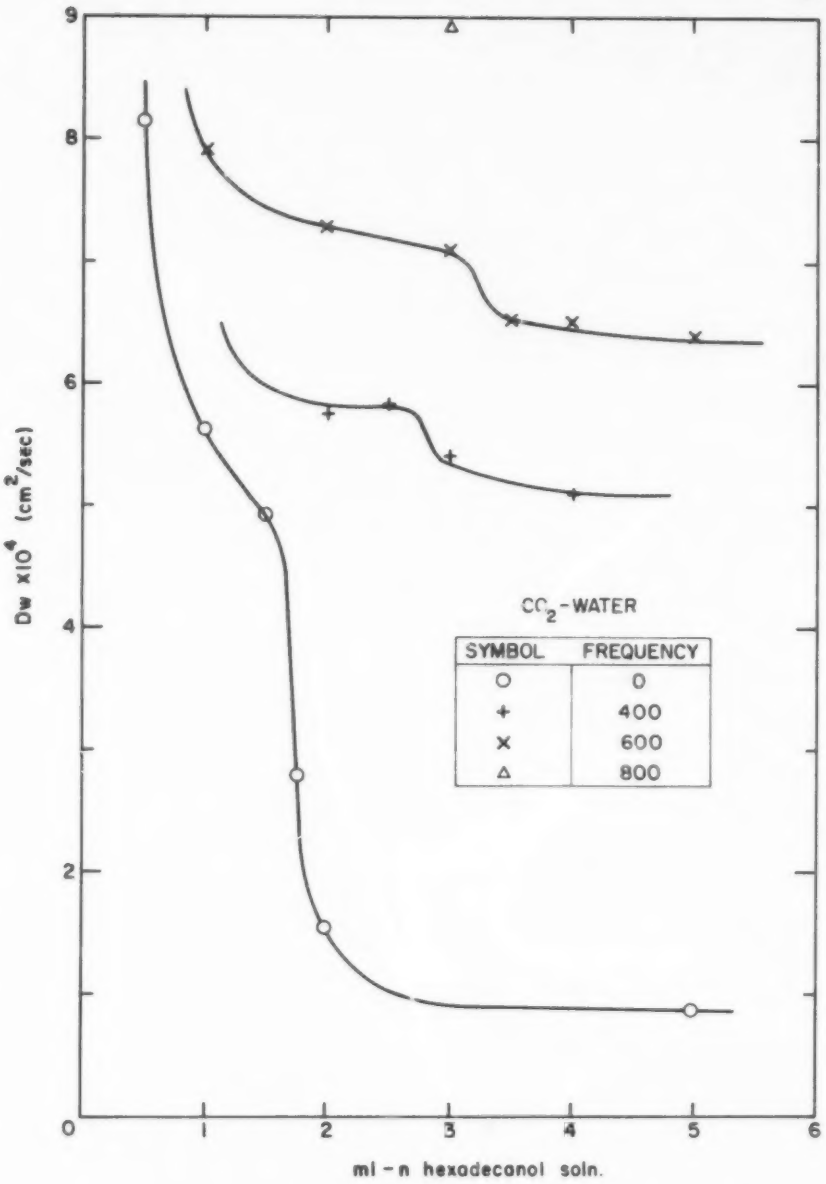

FIGURE 4-5 INFLUENCE OF MONOLAYER ON EFFECTIVE DIFFUSIVITY. SMALL FILM RESISTANCE

established for any other frequency by obtaining only a few points on Figure 4-4 or 4-5. In this manner, the monolayer for 800 cpm would appear to be established around four and one quarter milliliters.

For the no wave runs, the data approached a value of four times that of the molecular diffusivity when the surface was covered. This tends to imply that the action of the monolayer dampens or separates the fluid motion from the absorbing layer. Without the monolayer, D_w values were forty times the molecular value. The presence of the monolayer reduced D_w by a factor of nearly ten times those obtained for a clean surface. This reduction supports the Marangoni instability assumption, as the perturbations in surface concentrations which cause changes in surface tension are retarded by the monolayer, and the turbulent aspects of the diffusion coefficient are nearly removed.

When surface motions are employed by producing waves at various frequencies, there are sizeable increases in D_w values. This would support the motion of the fluid particles in the wave surface as the cause of this increase. This motion may cause the gas phase to contact the liquid phase directly rather than diffusing through the entire monolayer. It is also possible that the surface area increase stretched the monolayer at the peaks of the waves, thus lessening the resistance to absorption.

Because some question exists regarding the values of k and m used to calculate D_w, two limits were investigated.

The literature value of k and m result in D_w values that are within a few percent of the lower or no film values. The upper limit values of D_w were calculated for comparison. These correspond to the case where the film offers a high resistance to mass transfer. This would be in keeping with the theoretical estimates of k made by Goodridge and Robb (17). These D_w values are given in Table 4-3 and Figure 4-5.

For the case when no waves were present, the data approached the value of the molecular diffusivity for a covered surface. This further supports the conclusion that Marangoni instability is the dominant mechanism. The rest of the data trends are essentially the same as in the previous case, except that the D_w values are smaller.

Evaporation Considerations: During the course of the experimental part of this dissertation, the adaption of the experimental apparatus used for the absorption study was considered for an evaporation study. Using the mathematical model in Chapter II, Equation (2-41), it was found that the time necessary to obtain fifty percent saturation was somewhat less than fourteen seconds. Thus if the experimentation was performed following the procedure used in the absorption study, most of the evaporation would have taken place before the ball valves could be closed and data recorded. To accomplish an accurate study of an evaporation procedure, a steady state method would be necessary rather than the unsteady system used for absorption.

CHAPTER V

CONCLUSIONS

Theories have been established for diffusion in a gas-liquid system such as that of carbon dioxide-water reported in this dissertation. However, they do not consider the presence of surface waves on the transfer interface, nor do they account for the turbulence that occurs within the fluid body. Practical applications of wave study stem from a qualitative correction of the diffusion coefficient. These coefficients can be applied to two phase systems which utilize either absorption or evaporation, and exhibit wave phenomena at the gas-liquid interface.

Retardation of evaporation and absorption are of great interest. Water reservoirs which store millions of gallons of water, daily lose substantial amounts to the atmosphere through evaporation when wind produces waves on the water surface. Many other practical applications may be applied to the retardation of absorption or evaporation. A study of effective materials to accomplish this and the models that govern transfer is surely a rewarding contribution to the field of chemical engineering.

During the course of this investigation the liquid surface depth in the ripple tank was varied between 5.08 and 0.635 centimeters. The effective diffusivity of a carbon dioxide-water system was found for each of these depths. A

clean surface, free from any foreign material was utilized in this portion of the analysis. Waves were produced at frequencies of 400, 600, and 800 cycles per minute. It was found that the effective diffusivities obtained were much greater than those for molecular diffusion. Possibly an increase in liquid surface area or natural convective turbulence in the body of the fluid were responsible for this increase. Since very small waves were used it is believed that the contribution of increased surface area to the diffusion coefficient was small. Most of the increase is attributed to the natural convection produced by buoyant effects, or Marangoni instability. Heat of solution was considered, but discarded, because the temperature produced from it was negligible. As the liquid depth was decreased, so the effective diffusivity decreased. As eliptical motions of the fluid directly under the waves flattened with decreasing depth, fluid motion was decreased.

In the monomolecular film case, the effectivity diffusivity was determined at wave frequencies of 400, 600, and 800 cycles per minute. Measurements were made for various amounts of n-hexadecanol solution on the liquid surface. The application of this layer reduced the effective diffusivity by a factor of five to thirty times the original value. Until the surface had enough surface active agent to completely cover it, no model could describe its behavior. In the no wave case, the effective diffusivity determined approached the value of molecular diffusion, or 2.0×10^{-5} cm^2/sec.

This result shows that fluid motion in the liquid phase was due to Marangoni instability, as perturbations in surface concentration caused changes in the surface tension, which in turn produced secondary fluid motions. In effect the addition of the monolayer masked the natural convection motion of the liquid bulk, which decreased the numerical value of the effective diffusivity. Practically speaking, the decreasing of the absorption coefficient by a factor of thirty can be considered a successful step in retardation of liquid losses.

Evaporation was considered in this analysis, but because of experimental difficulties, data could not be obtained using the scheme devised in this dissertation. In future analysis, a steady state system may solve this difficulty, and a complete analysis may be made for evaporation through reproducible wave motions. It may be of future interest to study the mass transferred in a simple life cycle as that associated with algae. It may also be of interest to examine a kinetic study accompanying mass transfer in reproducible wave motions.

APPENDIX A

LISTING OF DATA AND TABULATED QUANTITIES

Table A-1 through A-S1

APPENDIX A

CLEAN SURFACE CASE

Tables* A-1: Liquid Depth - 1/4"

Total Moles Absorbed

Time (sec.)	0 cpm Frequency	600 cpm Frequency
240	.00326	.00396
900	.0093	.0118
1380	.0124	.0150
2400	.0174	.0226
3600	.0219	.0297
4800	.0259	.0352
6000	.0293	.0394
7200	.0315	.0428

Tables A-2: Liquid Depth - 1/2"

Total Moles Absorbed

Time	0 cpm	400 cpm
300	.00465	.00402
1200	.0124	.0124
2400	.0196	.0216
3000	.0223	.0254
4200	.0265	.0324
5400	.0292	.0379
6600	.0308	.0422

Time	600 cpm	800 cpm
120	.00239	.00248
600	.0080	.0084
1200	.0138	.0149
2400	.0237	.0256
3600	.0316	.0340
4800	.0377	.0403
6000	.0428	.0455
7200	.0467	.0495

---

*The data in Tables A-1 through A-M4 represent only a sample of the total data obtained.

Tables A-3: Liquid Depth - 1"

Total Moles Absorbed

Time	0 cpm	600 cpm
120	.00225	.00247
600	.00738	.00874
1200	.0135	.0152
3000	.0278	.0330
4800	.0386	.0472
6600	.0473	.0585
7320	.0504	.0622

Tables A-4: Liquid Depth - 2"

Total Moles Absorbed

Time	0 cpm	600 cpm
120	.00165	.00124
600	.00716	.00637
1200	.0136	.0134
3000	.0303	.0323
4800	.0439	.0490
6050	.0522	.0590
7320		.0681

Tables A-5: Liquid Depth - 2"

No Gauze Enwrapped Dampers in Tank Ends
Total Moles Absorbed

Time	0 cpm
300	.00302
600	.00636
1200	.0126
2400	.0247
3600	.0359
4800	.0453
5400	.0494
6000	.0535

MONOMOLECULAR FILM CASE

Tables A-M1: 0 cpm Frequency - no wave

Amount of n-hexadecanol Solution

Time	1/2 ml	1 ml
120	.00138	.00121
600	.00459	.00389
1200	.00922	.00645
2400	.0185	.0112
3600	.0282	.0166
4800	.0376	.0233
6000	.0480	.0323
7200	.0546	.0429

Time	1-1/2 ml	1-3/4 ml
120	.00132	
600	.00384	.00398
1200	.00675	.00624
2400	.0120	.00985
3600	.0173	.0126
4800	.0239	.0167
6000	.0314	.0212

Time	2 ml	5 ml
120	.00114	.00135
600	.00372	.00340
1200	.00565	.00477
2400	.00872	.00695
3600	.0115	.00905
4800	.0130	.0104
6000	.0152	.0118
6600	.0164	.0125

Tables A-M2: 400 cpm Frequency

Amount of n-hexadecanol Solution

Time	2 ml	2-1/2 ml
300	.00246	.00252
600	.00443	.00417
1200	.00772	.0081
2400	.0158	.0161
3600	.0238	.0245
4800	.0313	.0323
6000	.0396	.0409

Tables A-M2 (Continued):

Time	Amount of n-hexadecanol Solution 3 ml	4 ml
300	.00255	.0024
600	.00402	.00414
1200	.00732	.00696
2400	.0151	.0138
3600	.0227	.0291
4800	.0305	.0301
6000	.0377	.0373

Tables A-M3: 600 cpm Frequency

Time	Amount of n-hexadecanol Solution 1 ml	2 ml
300	.00308	.00292
600	.00579	.00535
1200	.0115	.010
2400	.0238	.0196
3600	.0349	.0302
4800	.0450	.0405
6000	.0544	.050

Time	3 ml	3-1/2 ml
300	.00344	.00301
600	.00542	.00491
1200	.00923	.00855
2400	.0188	.0172
3600	.0286	.0256
4800	.0388	.0341
6000	.0483	.0426
7200	.0570	

Time	4 ml	5 ml
300	.0025	.00203
600	.00472	.00418
1200	.00834	.00755
2400	.0167	.0167
3600	.0254	.0258
4800	.0337	.0349
6000	.042	.0445

Tables A-M4: 800 cpm Frequency

Time	Amount of n-hexadecanol Solution 3 ml
300	.00304
600	.00625
1200	.0122
2400	.0242
3600	.0364
4800	.0477
6000	.0582
6600	.0633

Tables A-S1: CO_2 Solubility Data (24)

Substance	Temperature °C	Solubility α*
Carvol $C_{10}H_{14}O$	20	2.506
Isobutal Alcohol	25	1.694
Engenol $C_{10}H_{12}O_2$	20	1.54
Russian Petroleum	20	1.17
Transformer Oil	25	0.99

*α = Bunsen absorption coefficient equals volume of gas (reduced to 0°C and 760mm) which at temperature of experiment is dissolved in one volume of the solvent when the partial pressure of the gas is 760mm.

APPENDIX B

MISCELLANEOUS FIGURES

B-1 through B-4

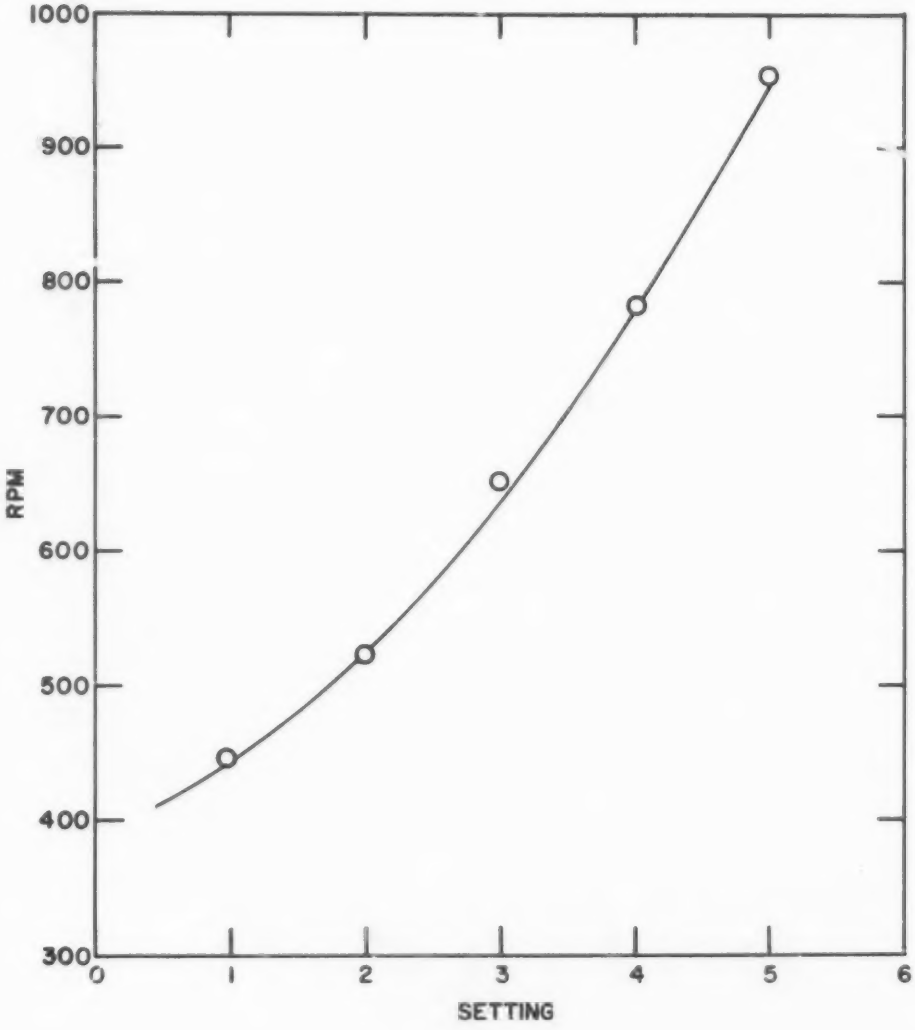

FIGURE B-1 CAM MOTOR SPEED

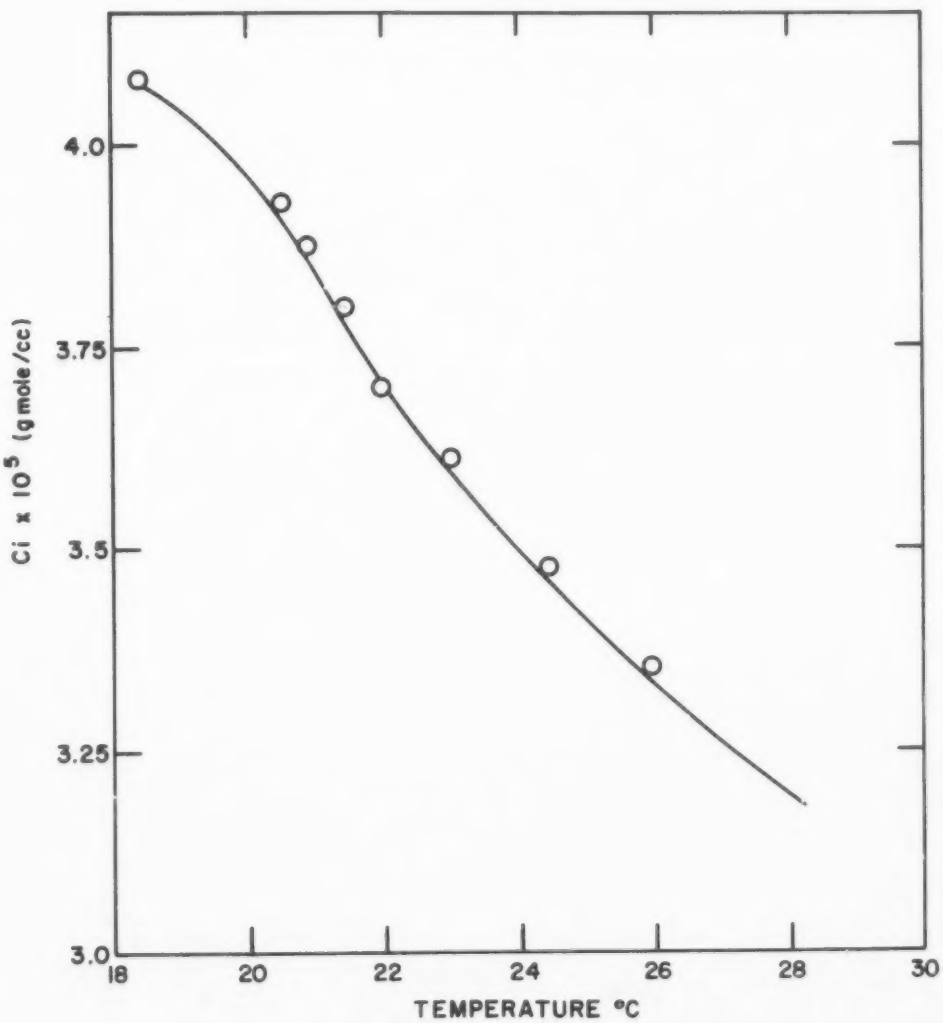

FIGURE B-2 SOLUBILITY OF CARBON DIOXIDE (24)

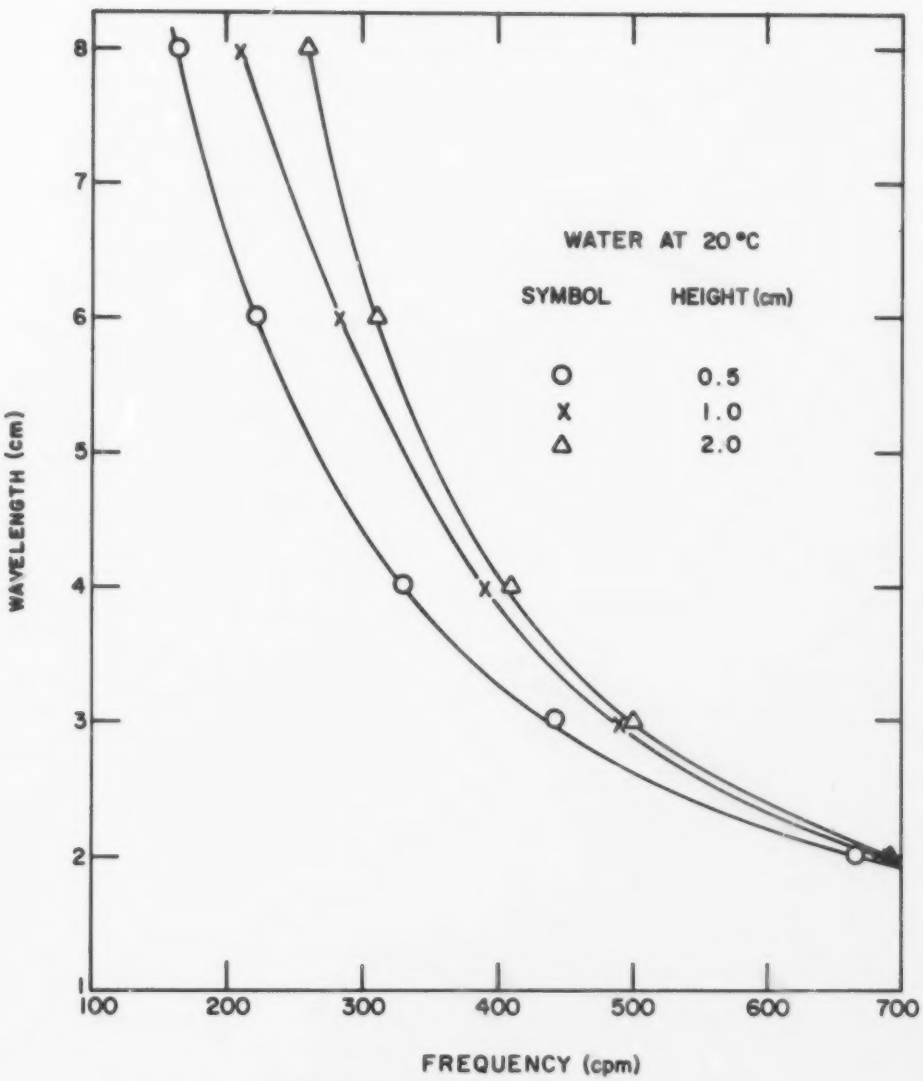

FIGURE B-3 WAVELENGTH-FREQUENCY RELATION

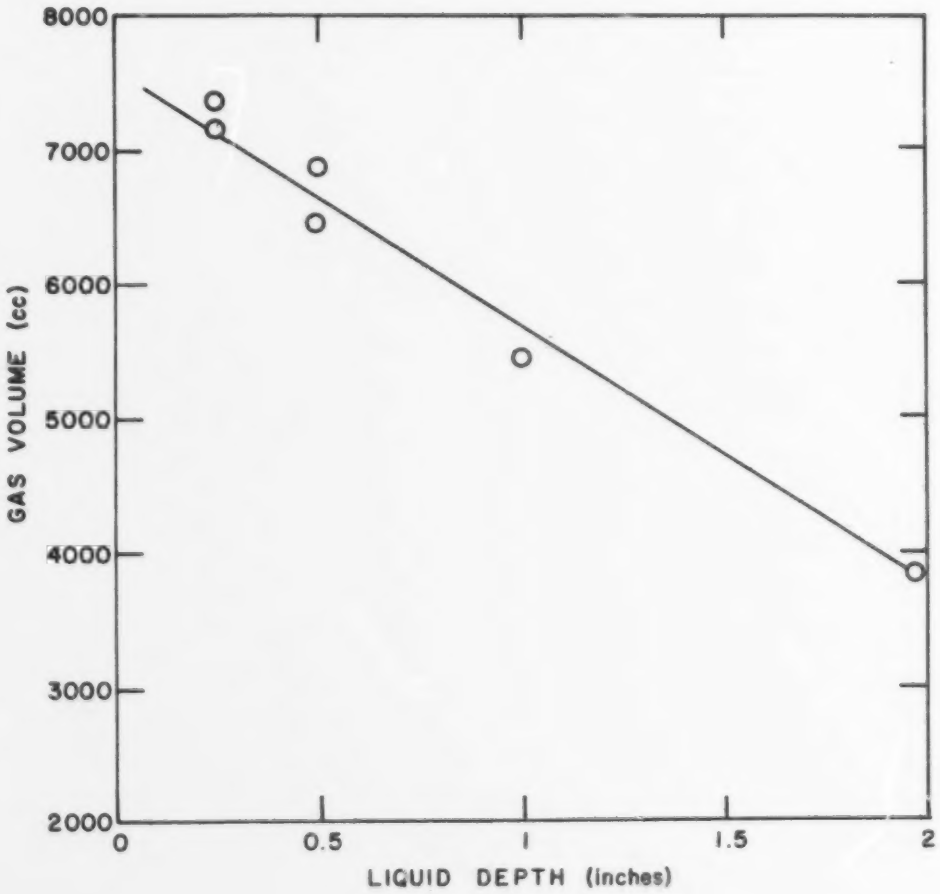

FIGURE B-4 RIPPLE TANK GAS VOLUME

NOMENCLATURE

A	Surface area, cm^2
α	Bunsen absorption coefficient
C	Concentration, $gmoles/cm^3$
$\overline{C}$	Concentration of carbon dioxide in monolayer, $gmoles/cm^3$
C'	Fluctuation component of concentration, $gmoles/cm^3$
$\overline{C}$	Average concentration in liquid at any time, $gmoles/cm^3$
C_i	Defined as m/H
C_i	Equilibrium concentration, $gmoles/cm^3$
C_p	Specific heat, cal/gmole °K
C_{sf}	Saturation concentration of film, $gmoles/cm^3$
C_{sw}	Saturation concentration of water, $gmoles/cm^3$
D	Molecular diffusivity, cm^2 /sec
d	Measured change in volume, cm^3
D_f	Film diffusion, constant, cm^2/sec
D_w	Effective diffusivity, cm^2/sec
δ	Film thickness, cm
ε	Eddy diffusivity, cm^2/sec
f	Frequency, cpm
H	Henry's law constant
h	Depth of liquid, cm
ΔH_s	Heat of solution, cal/gmole
$\overline{J}$	Total flux vector, $gmoles/cm^2$-sec
$\overline{J}_d$	Surface flux of dilute component due to molecular diffusion
$\overline{J}_f$	Surface flux of dilute component due to bulk flow

k	Pseudo steady state mass transfer coefficient
λ	Eigen valve
M	Molecular weight
m	Distribution coefficient
N	Defined as $-k/mD_w$
N	Transfer flux, gmoles-cm/sec
N_o	Avagadros number
n	Index for summation
$\bar{n}$	Outward unit normal vector
Δn	Total gas absorbed, gmoles
P	Gas pressure, atm
P_i	Defined as $-m/H$
r	Collision radius of molecule, cm
r_o	Liquid depth, cm
ρ	Density of solution
S	Control volume surface area, cm^2
Sl	Slope of $(1-n/C_iV_l)$ versus time
T	Temperature of gas space, °K
T_f	Final temperature, °K
T_i	Initial temperature of gas space, °K
T_o	Reference temperature, °K
θ	Time, sec
V	Gas volume, cm^3
v	Control volume of; liquid, cm^3
v'	Fluctuating component of velocity, cm/sec
V_{abs}	Absolute gas volume, cm^3
V_c	Corrected gas volume, cm^3

V_{gs}	Volume of gas space, cm^3
V_l	Liquid volume, cm^3
y	Verticle cartesian coordinate distance, cm, positive upward

LITERATURE CITED

1. Addison, C. C., Phil. Mag., 36, (7), 73 (1945)

2. Archer, R. J., LaMer, M. K., J. Phys. Chem. 59, 200 (1955)

3. Barnes, G., LaMer, M. K., Retardation of Evaporation by Monolayer, Transport Processes, p. 9, Academic Press, New York (1962)

4. Bird, R. B., Advances in Chem. Engr. Vol. I, p. 175, Academic Press (1956)

5. Bird, R. B., Steward, W. E., Lightfoot, E. N., Transport Phenomena, p. 645, John Wiley and Sons (1960)

6. Blank, M., Retardation of Evaporation by Monolayers, Transport Processes, p. 75, Academic Press, New York (1962)

7. Bond, J., Donald, M. D., Chem. Engr. Sci., 6, 237 (1957)

8. Brock, J. R., Bird, R. B., AIChE Journal, 1, 174 (1955)

9. Brooks, J. H., Retardation of Evaporation by Monolayers, Transport Processes, p. 259, Academic Press, New York (1962)

10. Carslaw, H. S., Jaeger, J. C., Conduction of Heat in Solids (2nd ed.), p. 100, Oxford Press (1959)

11. Chapman, J. A., The Effect of Small Surface Waves on Mass Transfer Rate, M.S. Thesis, Oklahoma State Univ. (1961)

12. Chiang, S. H., Toor, H. L., AIChE Journal, 5, 165 (1959)

13. Copeland, L. E., Harkins, W. D., Boyd, G. E., J. Chem. Phys. 10, 357 (1942)

14. Cullen, E. J., Davidson, J. E., Chem. Eng. Sci., 6, 49 (1956)

15. Dwight, H. B., Tables of Integrals and Other Mathematical Data, p. 82, The MacMillan Co. (1955)

16. Ferguson, A., Phil. Mag., 28, 403 (1914)

17. Goodridge, R., Robb, I. D., Ind. & Engr. Chem. Fund., 4, 49 (1965)

18. Grimley, S. S., Trans. Inst. Chem. Engrs. (London), 23, 229 (1945)

19. Hanratty, T. J., Engen, J. M., AIChE Journal, 3, 299 (1957)

20. Hanratty, T. J., Hershman, A., AIChE Journal, 7, 488 (1961)

21. Harkins, W. D., Copeland, L. E., J. Chem. Phys., 10, 272 (1942)

22. Harkins, W. D., Young, T. F., Boyd, G. E., J. Chem. Phys., 8, 954 (1940)

23. Hutchinson, M. H., Sherwood, T. K., Ind. Eng. Chem., 29, 836 (1937)

24. International Critical Tables, Vol. III, p. 254, McGraw Hill (1928)

25. Jackson, M. L., AIChE Journal, 1, 231 (1955)

26. Kimball, G. E., J. Chem. Phys., 6, 447 (1938)

27. King, J. L., Boyle, D., Ogle, J. B., J. Fluid. Mech., 4, 283 (1958)

28. Kuper, C. G., Trevena, D. H., Phys. Soc. Proc., 65, 46 (1952)

29. Lemlich, R., Levy, M. R., AIChE Journal, 7, 240 (1961)

30. Levich, V. G., Physiocochemical Hydrodynamics, p. 683-9, Prentice Hall (1962)

31. Lilleleht, L. V., Hanratty, T. J., AIChE Journal, 7, 548 (1961)

32. Lilleleht, L. V., Hanratty, T. J., J. Fluid. Mech., 11, 65 (1961)

33. Merson, R. L., Quinn, J. A., AIChE Journal, p. 804, Nov. (1964)

34. Muenz, K., The Effect of Small Surface Waves on Interfacial Mass Transfer, Ph.D. Thesis, Univ. of Maryland (1965)

35. Othmer, D. F., Gilmont, R., Petrol. Refiner, 31, 107 (1952)

36. Raimondi, P., Toor, H. L., AIChE Journal, 5, 86 (1959)

37. Rohsenow, W. M., Choi, H., Heat, Mass, and Momentum Transfer, pp. 113, 392, 506, Prentice Hall (1961)

38. Rosano, H. L., LaMer, V. K., J. Phys. Chem., 60, 348 (1956)

39. Schlichting, H., Boundry Layer Theory, p. 461, McGraw Hill (1960)

40. Scriven, L. E., Chem. Engr. Sci., 12, 98 (1960)

41. Scriven, L. E., Pigford, R. L., AIChE Journal, 4, 439 (1958)

42. Sternling, C. B., Scriven, L. E., AIChE Journal, 5, 514 (1959)

43. Striba, C., Hurt, O. H., AIChE Journal, 1, 178 (1955)

44. Tailby, S. P., Portalski, S., Chem. Engr. Sci., 17, 283 (1962)

45. Vivian, J. E., King, C. J., AIChE Journal, 10, 520 (1964)

46. Wilke, C. R., Prausnitz, J. M., Acrivos, A., Ind. Engr. Chem., 51, 466 (1959)